JBC Papers in Press. Published on August 25, 2015 as Manuscript M115.672121
The latest version is at http://www.jbc.org/cgi/doi/10.1074/jbc.M115.672121

The Potato Nucleotide-Binding Leucine-Rich Repeat (NLR) Immune Receptor Rx1 is a Pathogen Dependent DNA-Deforming Protein*

Stepan Fenyk[1,2], Philip D. Townsend[1,2], Christopher H. Dixon[1,2], Gerhard B Spies[1,2], Alba de San Eustaquio Campillo[1,2], Erik J. Slootweg[4], Lotte B. Westerhof[4], Fleur K.K. Gawehns[5], Marc R. Knight[1,2], Gary J. Sharples[1,2], Aska Goverse[4], Lars-Olof Pålsson[3], Frank L.W. Takken[5,6] and Martin J. Cann[1,2,6]

[1]School of Biological and Biomedical Sciences, [2]Biophysical Sciences Institute, [3]Department of Chemistry, Durham University, South Road, Durham, DH1 3LE, United Kingdom.

[4]Laboratory of Nematology, Department of Plant Sciences, Wageningen University, 6708 PB, Wageningen, The Netherlands,

[5]Molecular Plant Pathology, Swammerdam Institute for Life Sciences, University of Amsterdam, Science Park 904, 1098 XH, Amsterdam, The Netherlands.

[6] These authors contributed equally to this work

*Running title: *Rx1 is a DNA-deforming protein*

To whom correspondence should be addressed: Martin J. Cann, School of Biological and Biomedical Sciences, Durham University, South Road, Durham, DH1 3LE, United Kingdom. Phone: +44 (191) 3343985. Fax: +44 (191) 3341201. E-mail: m.j.cann@durham.ac.uk.

Keywords: Cellular immune response, DNA-binding protein, Host-pathogen interaction, Nod-like receptor, Plant biochemistry, Plant defence, Plant virus.

Background-Direct targets for plant NLR proteins in immune signalling are largely unknown.
Results-The Rx1 NLR protein of potato binds and distorts DNA following pathogen perception resulting in immune activation.
Conclusion-DNA is a direct signalling target for a plant NLR immune receptor.
Significance-Plant NLR receptors might regulate immune transcriptional responses by directly interacting with plant chromatin.

SUMMARY.
Plant NLR proteins enable cells to respond to pathogen attack. Several NLRs act in the nucleus, however, conserved nuclear targets that support their role in immunity are unknown. Previously we noted a structural homology between the NB domain of NLRs and DNA replication origin-binding Cdc6/Orc1 proteins. Here we show that the NB-ARC domain of the Rx1 NLR of potato binds nucleic acids. Rx1 induces ATP-dependent bending and melting of DNA *in vitro* dependent upon a functional P-loop. *In situ* full-length Rx1 binds nuclear DNA following activation by its cognate pathogen-derived effector protein, the coat protein of potato virus X. In line with its obligatory nucleocytoplasmic distribution, DNA-binding was only observed when Rx1 was allowed to freely translocate between both compartments *and* was activated in the cytoplasm. Immune activation induced by an unrelated NLR-effector pair did not trigger a Rx1-DNA interaction. DNA-binding is therefore not merely a consequence of immune activation. These data establish a role for DNA distortion in Rx1 immune signalling and defines DNA as a molecular target of an activated NLR.

Plants and animals possess innate immune systems enabling individual cells to mount a defence response upon pathogen perception (1-4). The NLR family of immune receptors perceive non-self and modified-self molecules inside host cells and mediate immune responses to invading microorganisms. Plant NLRs typically detect strain-specific pathogen effectors while the animal NLRs commonly recognize microbe- or damage-associated molecular patterns (3,5,6). The NLR families in both kingdoms belong to the STAND P-loop ATPases of the AAA+ superfamily whose multi-domain structure allows them to function simultaneously as sensor, switch, and response factor (7,8).

Plant NLRs are named after their central NB and C-terminal LRR domains. The N-terminus is

highly divergent; in plants this region typically encompasses CC or TIR domains (3). The NB domain of plant NLRs is commonly referred to as the NB-ARC domain and has been proposed to function as a molecular switch (8-10). The LRR confers pathogen recognition specificity and maintains the NLR protein in a signalling competent yet auto-inhibited state. Biochemical analysis of tomato I-2 and Mi-1, flax M and L6, and barley MLA27 revealed that the NB-ARC domain is ADP bound in the auto-inhibited state (11-13). LRR-mediated pathogen recognition is proposed to permit the exchange of ADP for ATP allowing the NB-ARC domain to adopt an activated or "on" state. ATP hydrolysis to ADP enables the "off" state to be re-established. Support for this model comes from studies where I-2 mutants defective in ATP hydrolysis *in vitro* are auto-activated *in vivo* and from an auto-active flax M mutant that preferentially co-purifies with ATP (12,13). Recently the NB sub-domain of rice Os2g_25900 and NB-ARC domains of maize Pollen-Signaling Protein (PSiP) and *Arabidopsis* Rpm1 were demonstrated to possess a nucleotide phosphatase activity compatible with the switch model (14).

Activation of animal NLRs typically triggers NB domain-mediated self-association resulting in the formation of a cytoplasmic signalling scaffold on which partners are activated due to their induced proximity (15). For plant NLRs, such partners have not been identified and a pivotal, yet unanswered, question concerns the nature of the downstream signalling component(s) and how these are activated by NLR proteins in their "on" state. The identity of the specific NLR subdomain that transduces a signal to such a downstream component is also unresolved. Whereas for Rx1 the NB subdomain of Rx1 induces cell death, the N-terminal TIR domains of L6 and RPS4 or the coiled-coil domain of MLA10 suffice to trigger cell death, suggesting that the signalling domain might vary for different NLRs or that they act as heterodimers (11,16-18). The location of the NLR signalling event is also the subject of increased scrutiny. Several NLR proteins including N, Mla10, and Rx1 have a dynamic nuclear-cytoplasmic distribution while RRS1-R is restricted to the nucleus dependent upon the presence of the PopP2 immune elicitor (19-23). Genetic screens for compromised NLR-mediated resistance identified genes encoding components of the nuclear pore complex (24), indicating involvement of nuclear transport in immune signalling. More direct proof for nuclear activity is the observed nuclear localization for barley MLA1 and MLA10, *Arabidopsis* RPS4 and SNC1, and the tobacco N protein (22,25-27). Redirection of nuclear-resident MLA10, N, RPS4, and SNC1 to the cytoplasm compromises their ability to activate immune signalling, suggesting a nuclear signalling target (19,22,26,28). The potato Rx1 protein, which confers PVX resistance, localizes to both cytoplasm and nucleus (23). The Rx1 N-terminus interacts with a member of the RanGAP2 family that controls nuclear-cytoplasmic trafficking through the nuclear pore (29). Together, these studies indicate that nuclear-cytoplasmic trafficking and compartmentalization are essential for NLR protein function and suggest distinct activities in different cellular compartments. Recent studies on *Arabidopsis* RPS4 and barley Mla10 showed that induction of cell death was associated with cytoplasmic localization, whereas nuclear localization of RPS4 was associated with local resistance responses (25,30). The presence of a WRKY DNA-binding domain in RRS1-R (21) and the association of Mla10 with both Myb and WRKY transcription factors (31) have led to the hypothesis that plant NLRs regulate transcription in the immune response (32). This notion is further supported by interactions between a SPL transcription factor and the tobacco N NLR protein, the interaction between the SNC1 NLR protein of *Arabidopsis* and the TPR1 transcriptional co-repressor, and the presence of BED DNA-binding domains in many plant NLRs (27,33-35).

Based on these observations, signalling from plant NLRs can be viewed from two perspectives that are not necessarily mutually exclusive. In the first perspective, activated NLRs may act as platforms from which signalling proteins promoting immune responses are permitted to function. Alternatively, NLRs may themselves have an additional biochemical activity, independent of their ATPase activity, required for direct activation of plant immunity. In support of the latter model we here demonstrate that the Rx1 NLR protein of potato is able to bind DNA *in vitro* and *in situ* and that its *in vitro* activity consists of bending and melting DNA. We further demonstrate that the interaction of Rx1 with DNA as observed *in situ* only occurs after its genuine activation by the coat protein of PVX virus.

EXPERIMENTAL PROCEDURES

Structural Modelling - Protein fold searches using the Phyre[2] protein homology/analogy recognition engine V 2.0 (36) were undertaken using amino acids 143-488 of Rx1 using both normal and intensive modelling modes. Similar structural homology was also detected using the SAM-T08,

HMM-based protein structure prediction server (37). All superpositions were performed using the SSM algorithm in Coot (38). Models of Rx1 based on Cdc6/Orc1 (PDB accession 2V1U) were made using Chainsaw within the CCP4 package (39), and sequence alignments generated by the Phyre[2] server. Side chain packing and energy minimization was performed using GalaxyRefine (40). Figures were generated using the PyMOL molecular graphics system (41).

Plasmids - A PCR product spanning residues 1-489 of Rx1 (http://www.ncbi.nlm.nih.gov/nuccore/AJ011801.1) was cloned into the *Nco*I and *Bam*HI sites of pET32c (pET32c-Rx1$_{1-489}$) and fitted with a hexa-histidine tag for affinity purification of recombinant protein. The oligonucleotides used to construct pET32c-Rx1$_{1-489}$ were 5' GCC CCA TGG CTT ATG CTG CTG TTA C 3' (sense) and 5' GGC GGA TCC TTA TGC ACA TGA ATT TTG ATC ACT C 3' (antisense). Mutant constructs were generated by site-directed mutagenesis. A PCR product corresponding to amino acids 177-339 of PSiP (http://www.ncbi.nlm.nih.gov/gene/542027) was cloned into the *Xho*I and *Nco*I sites of pRSET-B (pRSET-PSiP$_{177-339}$) and fitted with a hexa-histidine tag for affinity purification of recombinant protein. The primers used to construct pRSET-PSiP$_{177-339}$ were 5' GGC CTC GAG AAA GGC TGT GGG TGG CCT TG 3' (sense) and 5' GGC CCA TGG TCA CTT GAT TGC ACA ATA ATG CCC A 3' (antisense). A PCR product corresponding to amino acids 1-126 of histone H2B of *Arabidopsis thaliana* (http://www.arabidopsis.org/servlets/TairObject?type=locus&name=AT3G09480) was subcloned into the Gateway entry vector pDONR207 via BP recombinant reaction and transferred via LR reaction into the plant binary vector pK7WGF2 (pK7WGF2-H2B) to fuse the open reading frame (ORF) to an N-terminal green fluorescent protein (GFP) ORF. The primers used to construct pK7WGF2-H2B were 5' GGG GAC AAG TTT GTA CAA AAA AGC AGG CTA CAA CAA TGG CCATG GCA CCG AAG GCA GAG 3' (sense) and 5' GGG GAC CAC TTT GTA CAA GAA AGC TGG GTC AGA ACT GGT GAA TTT GGT G 3' (antisense). pBIN-35S based plasmids corresponding to NBARC-GFP, CC-NBARC-GFP, NBARC-LRR-GFP, GFP-LRR, CC-GFP, Rx1-GFP, GFP-NLS-Rx1, GFP-NES-Rx1, CP105, and CP106 are as described (23). Mutant constructs were generated by site-directed mutagenesis. Pto and AvrPto were expressed using a construct that contains 35S promoter-driven *Pto* and *avrPto* as described (42). For the construction of Rx1-4Strep a double STREPII-tag (43) (-asWSHPQFEKggWSHPQFEKts-) was created by annealing the oligonucleotides m-Str1 (5' GGC CGC TAG CTG GAG TCA CCC TCA GTT CGA GAA GGG TGG ATG GTC ACA TCC ACA ATT TGA AAA GAC TAG TTA AT 3') and m-Str2 (5' CTA GAT TAA CTA GTC TTT TCA AAT TGT GGA TGT GAC CAT CCA CCC TTC TCG AAC TGA GGG TGA CTC CAG CTA GC 3') and ligating the annealed oligonucleotides in between the *Not*I and *Xba*I of pRAP 35S:YFP-myc (23) replacing the sequence encoding the myc-tag. From the resulting pRAP::YFP-STR2 a fourfold STREPII-tag was generated by fusing the *Asc*I-*Spe*I 35S::YFP-STR2 with the *Nhe*I-*Pac*I STR2-Tnos segment in pRAP digested with *Asc*I-*Pac*I. In the resulting pRAP::YFP-STR4 vector GFP was replaced by Rx1 cDNA using the *Nco*I and *Not*I sites as described for pRAP:Rx-GFP (23). The expression cassette was excised using the *Asc*I and *Pac*I restriction sites and introduced into the expression vector pHYG (44). The expression vector pHYG-Rx1-4Strep was transformed to *Agrobacterium tumefaciens* strain MOG101 for plant expression.

Protein expression and purification - Protein corresponding to the NB-ARC domain of PSiP (amino acids 178-505; PSiP-NBARC) was generated as described previously (14).

A 10 mL culture of pET32c-Rx1$_{1-489}$ (Rx1$_{1-489}$ wild type and mutant proteins) in *Escherichia coli* C41(DE3) was grown overnight in Luria Broth supplemented with 100 μg mL^{-1} ampicillin at 37°C. This culture was diluted into 1 L Luria Broth supplemented with 100 μg mL^{-1} ampicillin and grown at 37°C to O.D.$_{600\ nm}$=0.7. The growth temperature was reduced to 22°C and growth continued to O.D.$_{600\ nm}$=1.0. Protein production was induced at 22°C for 16 h with 100 μM isopropyl-β-D-thiogalactoside (IPTG). Pelleted cells were washed with 50 mM Tris-HCl pH 8.5, 1 mM EDTA and the pellet resuspended in twice its volume of 50 mM Tris-HCl pH 7.5, 100 mM NaCl, 5 mM EDTA. Cells were centrifuged (2700 g, 30 min, 10°C) and the pellet resuspended in twice its volume of 50 mM Tris-HCl pH 7.5, 100 mM NaCl, 5 mM EDTA, 1% (v/v) Triton X-100. Cells were lysed by sonication (150 s), centrifuged (75,500 g, 60 min, 10°C), and inclusion bodies washed twice in 5 ml of 50 mM Tris-HCl pH 8.0, 100 mM NaCl, 5 mM EDTA, 1 % (v/v) Triton X-100. The final pellet was resuspended in 2 ml 50 mM Tris-HCl pH 9.0, 100 mM NaCl, 1 mM EDTA, 1 mM dithiothreitol, 8 M urea).

Material was incubated at 50°C for 20 min prior to centrifugation (20,000 g, 30 min, 15°C) and the pellet was discarded. The supernatant was dialyzed into 50 mM Tris-HCl pH 8.5, 100 mM NaCl, 7 M Urea and incubated with Ni^{2+}-nitrilotriacetic acid resin (Qiagen) for 60 min at 4°C. Resin was washed with 10 bed volumes buffer A (50 mM Tris-HCl pH 7.5, 400 mM NaCl, 20 mM $MgCl_2$, 0.25 mM imidazole, 7 M urea), 10 bed volumes buffer B (buffer A with 1.5 M NaCl, 20 mM imidazole) and 20 bed volumes buffer C (buffer B with 10 mM NaCl). Protein was eluted with 5-bed volumes elution buffer (buffer C with 200 mM imidazole). Protein was resuspended at 1 mg ml^{-1} in 50 mM Tris-HCl pH 8.5, 9.6 mM NaCl, 0.4 mM KCl, 2 mM $MgCl_2$, 2 mM $CaCl_2$, 0.5 M arginine, 0.4 M sucrose, 0.75 M guanidine-HCl, 1 mM glutathione, 0.1 mM reduced glutathione and incubated at 4°C for 1 h. Refolded protein was dialyzed into 20 mM Tris-HCl pH 7.5, 50 mM NaCl, 2 mM $MgCl_2$, loaded onto a monoQ anion exchange column (GE Healthcare) and eluted using a 50 mM to 1 M NaCl gradient. Peak fractions containing $Rx1_{1\text{-}479}$ protein were concentrated, dialyzed into 20 mM Tris-HCl pH 7.5, 150 mM NaCl, 2 mM $MgCl_2$ and loaded onto a Superdex 200 gel filtration column and peak fractions eluted in the same buffer.

pRSET-$PSiP_{177\text{-}339}$ (PSiP-NB) was expressed in *E. coli* BL21(DE3) *cya*::*kan* at 22°C for 16 h with 100 µM IPTG. Pelleted cells were washed with 50 mM Tris-HCl pH 7.5, 1 mM EDTA resuspended in 50 mM Tris-HCl pH 7.5, 250 mM NaCl, 100 µM EDTA, lysed by sonication (150 s), and the supernatant incubated with Ni^{2+}-nitrilotriacetic acid resin for 60 min at 4°C. Resin was washed with 10 bed volumes of buffer D (50 mM Tris-HCl pH 7.5, 400 mM NaCl, 5 mM imidazole, 100 µM EDTA), buffer E (buffer D with 1.5 M NaCl and 20 mM imidazole) and buffer F (buffer E with 40 mM NaCl). Protein was eluted with 5 bed volumes of buffer F containing 200 mM imidazole. PSiP-NB was subsequently purified by anion exchange chromatography as described previously (14).

Orc1-1 and Orc1-3 of *S. solfataricus* were expressed and purified as described previously (45).

For Rx1-4Strep *Agrobacterium tumefaciens* strain MOG101 was transformed with construct pHYG-Rx1-4Strep and grown to A_{600nm} 1.0 in 20 g L^{-1} sucrose, 5 g L^{-1} Murashige and Skoog basal salt mixture, 1.95 g L^{-1} MES, pH5.6, 200 µM acetosyringone. The two youngest fully expanded leaves of 5-6 weeks old *Nicotiana benthamiana* plants were infiltrated completely. Infiltration was performed by injecting the *Agrobacterium* suspension into a *N. benthamiana* leaf at the abaxial side using a 1 ml syringe. Leaf material was harvested after 48 hrs and ground in liquid nitrogen with mortar and pestle. Ground material was resuspended 1/10 (w/v) in 10% (v/v) glycerol, 50 mM Tris-HCl pH 8.5, 150 mM NaCl, 2 mM $MgCl_2$, 0.1% (v/v) Tween-20, 5 mM DTT, 0.02 g ml^{-1} Polyvinylpolypyrrolidone, 0.2 mg ml^{-1} Pefabloc SC protease inhibitor (Roche). Cell debris and PVPP were removed by centrifugation (20,000 g, 20 min, 4°C). The extract was passed through a Sephadex G25 column and the flow through supplemented with 5 mM DTT, 0.2 mg ml^{-1} Pefabloc SC protease inhibitor, and 20 µg ml^{-1} avidin. The extract was incubated with Streptactin superflow resin (IBA) at 4°C overnight. Resin was washed with 10-bed volumes wash buffer (10% (v/v) glycerol, 50 mM Tris-HCl pH 8.5, 150 mM NaCl, 2 mM $MgCl_2$, 0.1 % (v/v) Tween-20, 5 mM DTT). Protein was eluted with 2 bed volumes of wash buffer supplemented with 15 mM desthiobiotin. Purified protein was dialyzed into 20 mM Tris-HCl pH 7.5, 150 mM NaCl, 2 mM $MgCl_2$ before use.

Circular dichroism - Eighty µM protein was dialysed into ddH_2O at 4°C. The baseline CD spectra of blank sample (ddH_2O) and 1.7 µM protein were measured using a J-810 spectropolarimeter (Jasco) at 180-300 nm (20 nm min^{-1}). The averaged data of replicate blank spectra was subtracted from protein spectra and the data normalized to zero at 250 nm. The corrected CD spectra from 190-240 nm were analysed using CDPro (46). The protein database generating the lowest RMSD was used as the best approximation for secondary structure content.

Electrophoretic mobility shift assays - The oligonucleotides used for quantitative EMSA are derived from a series of oligonucleotides that enables a comparison of relative DNA-binding affinity to varying DNA topologies independent of DNA sequence (47). The oligonucleotides sequences were 5' TGG GTC AAC GTG GGC AAA GAT GTC CTA GCA ATG TAA TCG TCT ATG ACG TT 3' (SS1; DNA sense-strand), 5' AAC GTC ATA GAC GAT TAC ATT GCT AGG ACA TCT TTG CCC ACG TTG ACC CA 3' (SS2; DNA antisense-strand), and 5' UGG GUC AAC GUG GGC AAA GAU GUC CUA GCA AUG UAA UCG UCU AUG ACG UU 3' (RNA sense-strand) (47). Oligonucleotides were end-labelled with 10 µCi [γ-^{32}P]-ATP using T4 polynucleotide kinase and unincorporated nucleotides removed using Micro Bio-Spin columns (Bio-Rad). Protein and 0.15 nM nucleic acids (oligo 1-ssDNA, annealed oligo 1 and

oligo 2-dsDNA, and ssRNA) were incubated in 20 mM Tris-HCl pH 8.0, 60 mM NaCl (unless otherwise stated), 2 mM EDTA, 1 mM DTT, 10% (v/v) glycerol, 0.1 mg/ml BSA for 20 min on ice. Quantitative EMSAs were separated on a native 7% (w/v) polyacrylamide gel. Experiments to assess the role of nucleotides on DNA-binding used binding reactions and gels supplemented with 10 mM $ZnCl_2$ and nucleotide. Polyacrylamide gels were dried and analysed by autoradiography. EMSAs using unlabelled virion DNA were separated using 0.8% (w/v) Tris-acetate-EDTA agarose gels and stained with ethidium bromide. All reported values for K_d represent apparent K_d due to the potential for dissociation of protein-DNA complexes during electrophoresis. Curves were fitted by non-linear regression in GraphPad Prism 6.0.

Construction of DNA structures - DNA substrates corresponding to double-stranded branched structures (F12-ds/ds), branch structures with two single-stranded arms (F12-ss/ss) and branch structures with one double-stranded and one single-stranded arm (F12-ds/ss) were made by annealing synthetic oligonucleotides from a series that enables the comparison of relative DNA-binding affinity to varying DNA topologies independent of DNA sequence (47). Oligonucleotide sequences were 5' GAC GCT GCC GAA TTC TGG CTT GCT AGG ACA TCT TTG CCC ACG TTG ACC C 3' (SS3), 5' GCC AGA ATT CGG CAG CGT C 3' (LAG), 5' AAC GTC ATA GAC GAT TAC A 3' (LEAD). SS3 was end-labelled with 10 μCi [γ-^{32}P]-ATP using T4 polynucleotide kinase and unincorporated nucleotides removed using Micro Bio-Spin columns (Bio-Rad). SS3, SS1, LAG and LEAD were annealed to make F12-ds/ds. SS3, SS1 and LEAD were annealed to make F12-ds/ss. SS3 and SS1 were annealed to make F12-ss/ss. SS3 and the corresponding antisense oligonucleotide (5' GGG TCA ACG TGG GCA AAG ATG TCC TAG CAA GCC AGA ATT CGG CAG CGT C 3') were annealed to make a linear dsDNA control (dsF12) and SS3 used as linear ssDNA control (ssF12). Annealing synthetic oligonucleotides with a defined sequence mismatch made DNA substrates corresponding to linear DNA containing bubbles of defined length. Oligonucleotide sequences were 5' TTT GGT CTA ACT TTA CCG CTA CTA AAT GCC GCG GAT TGG TTT CGC TGA ATC AGG TTA TTA 3' (P1), 5' TAA TAA CCT GAT TCA GCG AAA CCA ATC CGC GGC ATT TAG TAG CGG TAA AGT TAG ACC AAA 3' (P2), 5' TAA TAA CCT GAT TCA GCG AAC CAA TCG CAA CCA TTT AGT AGC GGT AAA GTT AGA CCA AA 3' (P5), 5' TAA TAA CCT GAT TCA GCG AAA CAT TGT AGG TAA GCT TAG TAG CGG TAA AGT TAG ACC AAA 3' (P6) and 5' TAA TAA CCT GAT TCA GCG AAT GAC CGA TAA CGT CCA CTT GAG CGG TAA AGT TAG ACC AAA 3' (P7). P1 was end-labelled with 10 μCi [γ-^{32}P]-ATP using T4 polynucleotide kinase and unincorporated nucleotides removed using Micro Bio-Spin columns. P1 and P2 were annealed to make linear dsDNA (dsP1). P1 and P5 were annealed to make linear dsDNA with a 5-nucleotide bubble (dsP1-5). P1 and P6 were annealed to make linear dsDNA with a 13-nucleotide bubble (dsP1-13). P1 and P7 were annealed to make linear dsDNA with a 20-nucleotide bubble (dsP1-20). P1 was used on its own as a ssDNA control (ssP1). All substrates were gel-purified on a native 10% (w/v) polyacrylamide gel. EMSA was performed as described above.

ATPase assays - ATPase assays were typically performed at 37°C for 30 min with 2.3 μM protein in 50 mM 1,3-bis(tris(hydroxymethyl)methylamino) propane pH 7.5, 10 mM $MgCl_2$, and 5 μM ATP. Reactions were spiked with 0.5 μCi [2,8-^{3}H]-labeled ATP for quantitation. Reactions were spotted onto a silica thin layer chromatography plate with 1 mM ADP to act as marker and carrier. The plates were developed in isobutanol: 3-methyl-1-butanol: 2-ethoxyethanol: ammonia: H_2O (9:6:18:9:15). Spots were visualized at 256 nm and quantified using an AR-2000 TLC scanner.

Time-resolved FRET in vitro - Synthetic oligonucleotides, unlabelled or end labelled with fluorescein or tetramethylrhodamine (TAMRA), were purchased from Eurofins MWG. The oligonucleotides used were 5' TGG GTC AAC GTG GGC AAA GA 3' (sense-strand) and 5' TCT TTG CCC ACG TTG ACC CA 3' (antisense-strand). Strands were annealed by heating to 90°C for 3 min in 10 mM Tris pH 8.0, 1 mM EDTA before cooling to room temperature. Measurements used 1.5 μM protein with 50 nM DNA in the presence of 60 mM NaCl and were incubated for 10 min at room temperature before analysis. Time-resolved FRET was assessed using the Time-Correlated, Single Photon Counting (TCSPC) technique. The excitation source was a Picoquant pulsed diode laser LDH-P-C-485 (excitation wavelength 485 nm, 70 ps pulse FWHM at 20 MHz). Fluorescence was detected using an avalanche photodiode (Id Quantique 100-50) linked to a Becker and Hickl SPC 130 TCSPC module. An instrument response function of ~200 ps

was measured from Rayleigh scattered light. Fluorescence decays were collected for both donor and donor-acceptor labeled double-stranded DNA with or without protein using band pass filter detection of the donor emission and at magic angle polarization. Data was analyzed by the Grinvald-Steinberg method (48) to obtain the fluorescence lifetime for the donor and acceptor (τ_{DA}) and donor only (τ_D) labeled oligonucleotides. The data was fitted to a sum of exponentials using an iterative least squares re-convolution procedure with the optical/electrical excitation profile to produce a bi-exponential decay containing two lifetimes. This profile was obtained from a slide covered with Silica ludox particles, which provides an instant scatter of the excitation pulse. This data-fitting method provided more accuracy in the determination of shorter lifetimes than calculating a single average lifetime. Donor-acceptor distances (R) were calculated using the equation $E=R_0^6/(R_0^6+R^6)$ and a calculated Förster distance (R_0) of 49.99 Å. The total length of the oligonucleotide with linkers and fluorescent dyes, at maximum extension, was calculated as 81.1 Å.

P_1 nuclease sensitivity - Oligonucleotides for P_1 nuclease sensitivity were 5' CTC AAT ACA ATT GTC TCT GTG TAA ATT TCC TAC GTT TCA TCT GAA AAT CTA GCT ATT AGA GCT TGG TTT A 3' (sense-strand) and 5' TAA ACC AAG CTC TAA TAG CTA GAT TTT CAG ATG AAA CGT AGG AAA TTT ACA CAG AGA CAA TTG TAT TGA G 3' (antisense-strand) and represent the C3/mORB dual site sequence at *oriC2* of *Sulfolobus solfataricus* (49). The sense-strand oligonucleotide was end labelled with 10 μCi [γ-^{32}P]-ATP as described above and sense and antisense oligonucleotides annealed as required. Reactions were performed in 20 μl volumes containing 20 mM Tris-acetate pH 7.5, 10 mM magnesium acetate, 100 mM NaCl, 0.15 nM oligonucleotide and 1.5 μM protein. Protein was allowed to bind for 10 minutes at 37°C. P_1 nuclease was added to a final concentration of 0.01-0.1 U μl^{-1} and incubated for a further 20-60 min at 37°C. Reactions were stopped with 5 μl 100 mM Tris-HCl pH 8.0, 2.5% (w/v) SDS, 100 mM EDTA, 10 U μl^{-1} proteinase K. 5 μl of loading buffer (97.5% (v/v) formamide, 10 mM EDTA, 0.3% (w/v), 0.3% bromophenol blue) was added and reactions were electrophoresed on a 15% (w/v) polyacrylamide gel with 8 M urea. Polyacrylamide gels were dried and analysed by autoradiography.

Time-resolved FRET in situ - *Agrobacterium tumefaciens* strain GV3101 (pMP90) was transformed with constructs pK7WGF2 (GFP negative control), pK7WGF2-H2B (GFP-H2B positive control), pBIN35S-NBARC-GFP, pBIN35S-CC-NBARC-GFP, pBIN35S-NBARC-LRR-GFP, pBIN35S-GFP-LRR, pBIN35S-CC-GFP, pBIN35S-Rx1-GFP, pBIN35S-CP105 or pBIN35S-CP106 and grown to A_{600nm} 0.8 in YEB medium supplemented with 20 μM acetosyringone and 10 mM MES, pH 5.6. Cells were washed 3 times in infiltration medium (10 mM MES pH 5.6, 2% (w/v) sucrose, 20 μM acetosyringone) and infiltrated at A_{600nm} 0.4 into 4-5 week-old *N. benthamiana* leaves. Leaves were harvested after 72 hrs and prior to any observed cell death in a compatible immune interaction and the agroinfiltrated region was infiltrated with 10 μg/ml LDS 751 (Molecular Probes). For experiments with CP105 and CP106, the elicitor-encoding *A. tumefaciens* culture was infiltrated into pre-infiltrated sectors after 48 hrs (24 hrs before harvest). Leaves were fixed for 4 hrs at room temperature in 4% (w/v) paraformaldehyde in phosphate buffered saline (PBS). Fixative was quenched for 30 min at room temperature in 125 mM glycine and leaves washed in PBS at 4°C before mounting. A modified Zeiss Axiovert inverted epifluorescence microscope was used for time-resolved fluorescence microscopy. The overall excitation/detection of the fluorescence was performed using the time-correlated single photon counting technique. The excitation source was a Picoquant pulsed diode laser LDH-P-C-440 (excitation wavelength 440 nm, 70 ps pulse FWHM at 20 MHz). The objective lens (Zeiss 100x oil immersion Ph3) focused the excitation light on the sample material. The emission was detected using suitable band pass/long pass filters for GFP and LDS 751 fluorescence, respectively. Fluorescence was detected with a photon counting module (Id Quantique 100-50) in a single photon counting mode. Data fitting was performed as for time-resolved FRET *in vitro*. The relative orientation of the GFP tag does not affect Rx1 function (23) nor does it affect the ability to observe energy transfer. All data is reported for the analysis of GFP lifetimes as LDS 751 emission is influenced by photobleaching and variability in concentration.

Statistical analysis - Error bars represent the standard error of the mean with the number of replicates as indicated in the legend. Statistical comparisons (p values) for data that passes a test for normality (D'Agostino & Pearson omnibus normality test and Shapiro-Wilk normality test) were

obtained from one-way ANOVA with the indicated post-hoc test. Statistical comparisons (p values) for data that does not pass a test for normality were obtained from a Kruskal-Wallis test with post-hoc multiple comparisons test. P values in statistical comparisons are indicated in figures through letters and indicate compared data sets as described in the figure legends.

RESULTS

Plant NLRs are structurally related to Cdc6/Orc1 family proteins - The *Rx1* gene, introgressed in potato from the wild species *Solanum andigena*, confers resistance to PVX upon recognition of its coat protein (50,51). The Rx1 protein is a member of the CC-NB-LRR class of plant NLR proteins that consists of an N-terminal CC domain, a central NB-ARC domain and a C-terminal LRR domain. The NB domain, containing a central β-sheet flanked by α-helices, is flanked by two ARC subdomains. ARC1 forms a four-helix bundle, and ARC2 adopts a winged-helix fold characteristic of DNA-binding transcription factors (52). We hypothesized that an investigation of proteins structurally related to the Rx1 NB-ARC domain could provide insight into NLR biochemistry. Amino acids 143-488, encompassing the NB-ARC domain, were analysed using the Phyre[2] protein fold recognition engine and expected matches with the pro-apoptotic proteins CED-4 (PDB 2A5Y) and Apaf-1 (PDB 1Z6T) were recovered to 100% confidence (10,52). In correspondence with earlier structural studies (Tameling et al., 2006), high scoring matches (>99.4% confidence) were obtained with the Cdc6/Orc1 proteins of *Pyrobaculum aerophilum* (PDB 1FNN) and of *Aeropyrum pernix* in complex with DNA (PDB 2V1U). These proteins are members of a family of proteins involved in origin recognition and DNA replication in archaea and eukaryotes (45,49,53,54). NB sub-domain and tandem ARC domain residues (ARC1 and ARC2) of Rx1 are conserved between Cdc6/Orc1 of *A. pernix* and Rx1 (35.0% similarity and 12.7% identity between amino acids 134-479 of Rx1 and amino acids 13-382 of PDB 2V1U) (Figure 1A).

Both the N-terminal NB and C-terminal ARC domain-like regions of Cdc6/Orc1 contact DNA, inducing deformation of the double helix (45,49). The modeled tertiary structure of Rx1 (Figure 1B Left panel) was related to Cdc6/Orc1 bound to DNA (PDB 2V1U) (Figure 1B Centre panel), but differed from Cdc6/Orc1 in the DNA unbound state (PDB 1FNN) (Figure 1B Right panel). An overlay demonstrated that the difference between the modeled tertiary structure of Rx1 and Cdc6/Orc1 in the DNA unbound state (PDB 1FNN) was due to rotation of amino acids 279-388 of the C-terminal Cdc6/Orc1 ARC-like domain (Figure 1C Left and Centre panel). Amino acids 279-388 of the Cdc6/Orc1 C-terminal ARC-like domain can be excised from PDB 1FNN and directly superimposed onto the Rx1 ARC2 domain to demonstrate how this rotation has occurred in the absence of any global structural change (Figure 1C Right panel). Cdc6/Orc1 forms part of a larger family of structural homologues that includes the AAA+ ATPase SSO1545 from *Sulfolobus,* RuvB from *Thermus,* Orc2 from *Aeropyrum,* mammalian Apaf-1, CED-4 from *Caenorhabditis elegans* and NLRC4 from mouse (9,35,55-61). These proteins all show a similar domain arrangement of an NB domain that is coupled via its neighboring ARC1 domain to a C-terminal ARC2 domain with varying orientations. For example, the individual domains of the closed form of mouse NLRC4 (PDB 4KXF) can be extracted and superimposed onto Cdc6/Orc1 in the DNA bound state (PDB 2V1U) although their actual orientation does not support a DNA-binding activity. The modeled structural relationship with Cdc6/Orc1 suggests the intriguing possibility that Rx1 might also interact directly with DNA. We therefore investigated whether Rx1 is a DNA-binding protein.

Rx1 binds nucleic acids in vitro - A possible direct Rx1-DNA interaction was investigated through *in vitro* experiments. EMSA using nucleic acid fragments of >5 kb derived from circular bacteriophage ϕX174 (62) represents a straight forward methodology to qualitatively assess interactions between a protein and either single-stranded (ss) or double-stranded (ds) DNA with identical sequences. EMSAs were therefore performed using recombinant wild-type Rx1 protein ($Rx1_{1\text{-}489}{}^{WT}$), consisting of the CC-NB-ARC region but lacking the LRR domain (Figure 2A). EMSA experiments performed with the $Rx1_{1\text{-}489}{}^{WT}$ protein showed an association with both ssDNA and dsDNA, producing a small upward shift in the migration of the nucleic acid that is fully consistent with similar EMSA experiments using unrelated DNA-binding proteins (Figure 3A) (63). No mobility shift was observed with a control protein (BSA) that has a similar mass and isoelectric point as $Rx1_{1\text{-}489}{}^{WT}$.

The K176R mutation in the P-loop of Rx1 abolishes its ability to mount an immune response in the presence of the viral coat protein (23). The $Rx1_{1\text{-}489}{}^{K176R}$ loss-of-function mutant exhibited a barely detectable binding to DNA as compared to wild type Rx1 protein under these conditions (Figure 3A).

This difference is unlikely to be due to misfolding of the mutant as comparison of $Rx1_{1\text{-}489}^{WT}$ and $Rx1_{1\text{-}489}^{K176R}$ by circular dichroism (CD) reveals a generally similar secondary structure composition (Figure 2B-C). The CDSSTR method for secondary structure fraction prediction gave similar estimates for secondary structure content for both $Rx1_{1\text{-}489}^{WT}$ (61.6% helix, 14.8% sheet, 7.9% turn, 15.1% unresolved; NRMSD=0.066) and $Rx1_{1\text{-}489}^{K176R}$ (68.6% helix, 14.1% sheet, 7.9% turn, 8.7% unresolved; NRMSD=0.043) (64). Hence, subtle structural changes rather than an improperly folded protein likely explains differences in DNA-binding between $Rx1_{1\text{-}489}^{WT}$ and $Rx1_{1\text{-}489}^{K176R}$.

The Rx1-DNA interaction was relatively stable since it can be visualized after gel electrophoresis (Figure 3A). Nevertheless, while EMSA using circular bacteriophage ϕX174 DNA is a well-established method to qualitatively assess protein-DNA interactions, it does not enable robust quantification of the affinity of a protein for nucleic acids. EMSA with small synthetic oligonucleotides is a standard method to quantify protein-nucleic acid interactions (65). Furthermore, the high molecular weight of ϕX174 DNA and consequent small band shifts were not suited to further analysis. We therefore quantified the affinity of $Rx1_{1\text{-}489}$ for various nucleic acids by EMSA using ^{32}P-labelled synthetic oligonucleotides whose sequences were unrelated to that of bacteriophage ϕX174 DNA and which should provide more robust band shifts on EMSA due to their lower molecular weights (Figure 3A). $Rx1_{1\text{-}489}^{WT}$ showed broadly similar apparent affinities (K_d^{app}) for dsDNA and ssRNA but exhibited a significantly higher apparent affinity for ssDNA (Figure 3B-D; Table 1). The affinity of $Rx1_{1\text{-}489}^{WT}$ for dsDNA is within the sub μM range and is of a similar magnitude as both eukaryotic and prokaryotic Cdc6/Orc1 proteins (66,67). The apparent affinity of the $Rx1_{1\text{-}489}^{K176R}$ mutant for ssDNA, dsDNA and ssRNA was lower than the apparent affinity of wild type Rx1 in each case, which corresponds to the observed lower affinity established using the ϕX174 DNA (Akaike Information Criterion, $p>0.99$). To exclude the possibility that the observed nucleic acid binding was an artifact of the recombinant protein we purified full-length Rx1 protein from plants. Thereto the protein was purified using a C-terminal four-fold strep-tag (Rx1-4Strep) from agroinfiltrated *N. benthamiana* leaves. The amount of purified Rx1 protein obtained was limited but sufficient to demonstrate that plant-derived Rx1-4Strep is also able to bind to ssDNA *in vitro* (Figure 3E). Plant-derived Rx1-4Strep DNA-binding was weaker than that of bacterially derived protein, which could be due to the fact that the majority of the full-length Rx1 is presumably in the autoinhibited off-state. Only a small fraction is proposed to be spontaneously active and thought to be responsible for the weak HR phenotype observed when Rx1 is overexpressed in the absence of the CP elicitor (68). In addition, it cannot be excluded that the tag has impacted folding of a portion of the plant-expressed Rx1 protein.

The NLR NB-ARC domain binds nucleic acids in vitro - Despite the structural relationship between the Rx1 NB-ARC domains and Cdc6/Orc1 proteins, it is formally possible that the data of Figure 3 can be explained by an interaction between nucleic acids and the N-terminal CC domain of $Rx1_{1\text{-}489}$ rather than its NB-ARC domain. We were unable to produce truncated Rx1 fragments encompassing solely the NB or NB-ARC domains. We therefore examined another plant NLR protein to assess whether the NB-ARC domain alone is able to bind nucleic acids and whether DNA-binding is unique to Rx1 or represents a common property of at least a subset of plant NLRs. The NLR sub-domains of the orphan NLR of the monocot *Zea mays* were chosen as both the NB and NB-ARC domains can be produced as soluble recombinant protein (14). We compared ssDNA binding of the NB sub-domain of PSiP alone (PSiP-NB) to that of the complete NB-ARC domain of PSiP (PSiP-NB-ARC) (Figure 3F). Although both fragments bound, the PSiP-NB-ARC domains bound ssDNA with a considerably higher affinity than the PSiP-NB domain alone (Table 1). Together, these data demonstrate that the NB-ARC domain is sufficient for nucleic acid binding in Rx1 and PSiP, that DNA-binding is a property of at least a subset of plant NLR proteins, and that both the NB and the ARC sub-domains contribute to the DNA interaction.

Rx1 deforms DNA - In the 'switch' model for plant NLR activation, binding of ATP to the NB-ARC domain establishes the 'on' state while hydrolysis of ATP to ADP restores the 'off' state (9). An intact P-loop is essential for nucleotide-binding and mutations in this motif typically result in loss-of-function alleles (9). We therefore investigated the relationship between P-loop-dependent ATPase activity and DNA-binding. We detected no ATPase activity in $Rx1_{1\text{-}489}^{WT}$ possibly indicating the absence of a catalytic water molecule as previously observed for the STAND ATPase Ced-4 (69). Neither ATP nor ADP had any discriminatory influence on $Rx1_{1\text{-}489}$ binding to dsDNA (Figure 4A). We therefore

investigated whether Rx1 has activities at DNA other than binding that are affected by the type of nucleotide (ATP/ADP) bound. The Cdc6/Orc1 family proteins ORC1 of *A. pernix* and the Orc1-1/Orc1-3 heterodimer of *Sulfolobus solfataricus* substantially deform origin DNA by bending it with angles of 35° and 20° respectively, thereby inducing localized melting of the double helix (45,49,70). We therefore examined whether $Rx1_{1\text{-}489}$ can deform DNA in a similar fashion, and whether this process is nucleotide-type dependent. To measure DNA bending time-resolved FRET was used as it allows measurements of distances between fluorophores. This method offers considerable advantages over steady-state FRET as the fluorescence lifetime represents an intrinsic property of the fluorophore and is independent of concentration, photobleaching or light scattering (71). We monitored DNA deformation using time-resolved FRET with dual end-labeled dsDNA (72). Upon FRET the fluorescence lifetime of the donor fluorophore decreases and therefore we deconvoluted the fluorescence donor emission for its constituent lifetime components. We hypothesized that following DNA bending we would observe a shortened donor lifetime due to energy transfer to the acceptor. DNA bending was assessed under conditions to saturate binding of $Rx1_{1\text{-}489}^{WT}$ or $Rx1_{1\text{-}489}^{K176R}$ to dsDNA. Bending was evident as a decrease in the contribution of a 4.1 ns component (indicative of unperturbed donor emission; fluorescein fluorescence) and the appearance of a 129 ps component to the total fluorescence decay of FRET donor emission (Figure 4B, the 129 ps component is marked with an arrow). The 129 ps lifetime component, attributed to energy transfer, was only observed for the $Rx1_{1\text{-}489}^{WT}$ protein and $Rx1_{1\text{-}489}^{K176R}$ protein and not in controls without protein or with BSA except for a minor contribution with the latter in the presence of ATP (Figure 4C). The 129 ps lifetime corresponds to a calculated donor-acceptor distance of 29 Å (assuming isotropic orientations) and therefore an overall bend angle of 42° around a presumed oligonucleotide midpoint.

Next, it was investigated whether nucleotides had an influence on the observed DNA bending. Notably ATP, but not ADP, strongly increased the contribution of the 129 ps lifetime to the overall time-resolved data. This increase was only observed for the $Rx1_{1\text{-}489}^{WT}$ protein and not for the $Rx1_{1\text{-}489}^{K176R}$ mutant indicating that DNA bending requires an intact P-loop capable of binding nucleotides. The distinct response of the $Rx1_{1\text{-}489}^{WT}$ protein following incubation with either ADP or ATP provides additional support for a correct native fold of the nucleotide-binding pocket in the recombinant protein. The absence of any change in the value of the shortened lifetime (129 ps) shows that the calculated donor-acceptor distance is constant. As the relative proportion of the 129 ps lifetime to the total fluorescence signal increases in the presence of ATP and $Rx1_{1\text{-}489}^{WT}$, we can conclude that ATP binding enhances the pool of protein-DNA complexes in the bent state but not the bending angle.

Time-resolved FRET is a well-validated method to examine intra-molecular distances, and therefore DNA topology, but it does not provide further information on other DNA distortions associated with changes in topology. To examine whether $Rx1_{1\text{-}489}$ can induce local DNA melting, as has been observed for Orc1, we explored a non-fluorescent-based methodology. P_1 nuclease has previously been used as a tool to examine local DNA distortion using the Orc1 protein of *Aeropyrum pernix* (70). We therefore examined the sensitivity of dsDNA oligonucleotides to the ssDNA-specific P_1 nuclease in the presence of $Rx1_{1\text{-}489}$ (73). As expected, ssDNA was significantly degraded by P_1 nuclease (positive control) whereas dsDNA, in the presence of BSA (negative control), was largely resistant to P_1 nuclease activity (Figure 5). While dsDNA was more sensitive to P_1 nuclease in the presence of $Rx1_{1\text{-}489}$, the mutant $Rx1_{1\text{-}489}^{K176R}$ did not induce local DNA melting as no increased DNA degradation was observed. So, although in the *absence* of nucleotides $Rx1_{1\text{-}489}^{K176R}$ bends dsDNA to a similar magnitude to $Rx1_{1\text{-}489}^{WT}$, its failure to melt DNA might be a manifestation of subtle changes to DNA-binding evidenced through the decrease in binding affinity (Figure 3B-D). These experiments were insufficiently sensitive to examine the further influence of nucleotides on NLR-mediated DNA melting. The P_1 sensitivity of dsDNA in the presence of Orc1-1/Orc1-3 was indistinguishable from that of dsDNA in the presence of $Rx1_{1\text{-}489}^{WT}$ supporting the interpretation that plant NLRs can cause local dsDNA melting. In conclusion, Rx1 is able to both bend DNA and provoke local DNA melting, and this bending activity requires an intact P-loop and is stimulated by the presence of ATP.

Rx1 preferentially binds specific DNA topologies in vitro - We sought independent experimental support for Rx1-mediated distortion of DNA. We hypothesized that if Rx1 distorts linear DNA then the free energy of Rx1 binding to DNA structures that resemble the distorted state would be favored (with a corresponding increase in affinity). Indeed,

Rx1-bound branched double-stranded DNA with a significantly higher affinity than control linear double-stranded DNA of similar sequence (Figure 6A; compare dsF12 to F12-ds/ds). The branched double-stranded DNA represents a non-natural DNA and is a control to demonstrate a preference for $Rx1_{1\text{-}489}$ binding to a branched topology. When comparing binding affinities for naturally occurring branched topologies we noted a higher affinity for branched structures with one dsDNA and two ssDNA arms (e.g. similar to a transcription bubble) compared to structures with one or two duplex arms (e.g. resembling a DNA replication fork) (Figure 6A; compare F12-ds/ss to F12-ss/ss). Consistent with our model of local DNA melting, $Rx1_{1\text{-}489}$ showed a higher affinity for small DNA bubbles compared to linear dsDNA (Figure 6B). This increased affinity was not due to the increased affinity for ssDNA, as affinity did not correlate with increasing DNA bubble size. Although these data cannot reveal the exact nature of the distorted DNA state on DNA bending (Figure 4) and melting (Figure 5), analysis of the relative affinities does demonstrate that Rx1 shows an increased affinity for specific DNA structures and the DNA distortion we observed in the presence of Rx1 is likely a genuine response following its activation.

Rx1 DNA-binding is specifically activated by its cognate elicitor in vivo – DNA-binding, bending and melting is a new aspect of plant NLR biochemistry. To validate DNA as a downstream target for NLR signalling, and link this biochemical activity to its function in plant cells, we tested whether Rx1 is able to interact with DNA *in vivo*. To investigate the possibility of a direct interaction with genomic DNA inside the cell we studied Rx1-DNA interactions in the nucleus using Forster Resonance Energy Transfer-Fluorescence-Lifetime Imaging Microscopy (FRET-FLIM). FRET-FLIM has been previously used to demonstrate transcription factor binding to DNA in response to environmental signals (74).

N. benthamiana was infiltrated with *A. tumefaciens* carrying constructs encoding either GFP (negative control), a protein consisting of *A. thaliana* histone H2B fused to GFP (GFP-H2B; positive control), or discrete domains of Rx1 fused to GFP. Previous work has similarly utilized H2B-GFP and naked GFP as controls for DNA-binding in paraformaldehyde-fixed preparations (74). The constituent fluorescence lifetimes for the GFP tag were examined in leaves counterstained with LDS 751. LDS 751 is a cell permeable nucleic acid stain with an excitation maximum, when bound to DNA, which overlaps with the GFP emission spectrum. GFP showed two distinct lifetimes at ~0.5 and 1.5 ns (Figure 7A). Since energy transfer from donor (GFP) to acceptor (LDS 751) decreases the fluorescent lifetime, we hypothesized that the shorter lifetime for GFP is representative of energy transfer consistent with an interaction between the fluorophores. Notably, such a decrease in the GFP fluorescence lifetime by time correlated single-photon counting is independent of protein expression levels, quenching, photobleaching or fluctuations in the excitation source. A decrease in lifetime can therefore specifically be attributed to quenching of the excited state of the GFP and represents strong evidence for energy transfer from GFP to LDS 751 and thus a direct protein-DNA interaction. Consistent with this interpretation, a significant decrease in the ratio of the yields of the GFP fluorescence lifetimes was observed for the DNA-binding protein GFP-H2B (Figure 8A). To demonstrate that energy transfer to LDS 751, and not to surrounding proteins, explains the data we confirmed that the decrease in the fluorescence GFP lifetime ratio indicative of DNA-binding was correlated with an increase in LDS 751 emission that does not arise from the excitation source (Figure 7B). While the exact stoichiometry of GFP and LDS 751 levels is not known in each experiment, the finding that the ratio of fluorescence emission for GFP:LDS 751 is significantly decreased for H2B compared to the negative control is strong evidence that the reduction in GFP lifetimes is due to energy transfer to LDS 751 and not to an alternative molecule. As predicted, Rx1-GFP fusions containing the NB-ARC domain (NB-ARC-GFP, CC-NB-ARC-GFP, NB-ARC-LRR-GFP) showed a significant decrease in the ratio of GFP lifetime yields, consistent with its observed DNA-binding activity *in vitro*, while the LRR (GFP-LRR) domain did not. Surprisingly, the CC domain alone (CC-GFP) also showed a decrease in the ratio of GFP lifetime yields. The Rx1 CC domain has previously been shown to associate with a high molecular weight complex in the nucleus (23) and our findings indicate that this complex likely contains genomic DNA. Taken together, these data demonstrate that the CC and CC-NB-ARC Rx1 domains can form a stable interaction with DNA *in situ.* The FRET-FLIM methodology used is independent of expression levels of the various constructs. However, the methodology can be sensitive to cleavage of the GFP tag of even a small percentage of expressed protein. Fortunately, cleavage of the GFP tag can be resolved as it yields a *high*, rather than the observed *low* ratio of fluorescence lifetimes,

allowing us to conclude that the positive results for DNA-binding *in situ* are not attributable to tag cleavage.

Next, we investigated whether the full-length Rx1 molecule (Rx1-GFP) also binds to DNA in the plant cell. Notably, a full-length Rx1-GFP fusion showed no binding to DNA as compared to the negative control (Figure 8B). This implies that the inactive full-length Rx1 protein adopts a structure refractory to interacting with DNA. To test whether there is a relationship between DNA-binding and Rx1 activation and subsequent immune signalling we next co-expressed Rx1 with the PVX coat protein elicitor, which is known to trigger immunity (23). Full-length Rx1-GFP was found to bind to DNA only in the presence of the wild type (avirulent) coat protein (CP106) and not in the presence of a mutant (virulent) elicitor (CP105) that is unable to activate Rx1 (Figure 8B). These data show that DNA-binding *in vivo* by Rx1 only occurs upon perception of its cognate elicitor.

To test whether DNA-binding *in situ* requires elicitor recognition in the cytoplasm we investigated DNA-binding of Rx1-GFP fused to either a NLS or a NES. These chimeric tags have previously been demonstrated to constrain Rx1 to the nucleus or cytoplasm, respectively (23). This experiment addresses two-questions; 1) is enforced nuclear accumulation of a GFP fusion protein sufficient to confer DNA-binding and 2) at what subcellular localisation can Rx1 be activated by the coat protein to permit DNA-binding? GFP-NLS-Rx1 did not bind DNA in the presence or absence of CP106 demonstrating that enforced Rx1 accumulation in the nucleus is insufficient to drive DNA-binding *and* that DNA-binding requires CP106 recognition in the cytoplasm, consistent with previous findings (23) (Figure 8C). GFP-NES-Rx1 also did not bind DNA in the presence or absence of CP106 demonstrating that the DNA-binding signal is dependent on the ability of the cytosolic Rx1 protein to gain access to genomic DNA regardless of exposure to CP106. GFP-NES-Rx1 and GFP-NLS-Rx1 are not sensitive to cleavage of GFP thus excluding the possibility that the observed absence of DNA-binding is due to sensitivity to proteolysis (23). Taken together, the data support a model where Rx1 binding to DNA is a specific nuclear event in immune activation subsequent to coat protein detection in the cytosol.

We further investigated binding of Rx1-GFP to DNA upon activation of another immune receptor to exclude the possibility that Rx1 binds DNA as a non-specific consequence of defence activation. We co-infiltrated *N. benthamiana* with *A. tumefaciens* carrying constructs encoding Rx1-GFP, the Pto kinase of tomato and the AvrPto effector. The Pto kinase activates an immune response in *N. benthamiana* upon binding the AvrPto effector of *Pseudomonas syringae* pv.tomato (75-77). Rx1-GFP did not bind DNA when Pto was activated by AvrPto indicating that Rx1-GFP DNA-binding is not a generic response following defence activation (Figure 8D). As the role of Rx1 in immunity is dependent upon both its activation by the viral coat protein in the cytoplasm and its DNA-binding activity in the nucleus, our findings therefore provide the first evidence for a direct molecular target between activation of a plant NLR and subsequent cellular immune responses.

DISCUSSION

The molecular mechanism underlying the function of activated NLR proteins in plant immunity is a crucial, but still unanswered, question. Existing *in vitro*, *in vivo* and bioinformatics data pinpoint the NB-ARC domain as a central switch in regulating NLR activity. We here propose that the NB-ARC domain also possesses an intrinsic DNA-binding activity and we demonstrate that its DNA binding activity is associated with the cellular immune response. The Rx1 protein is observed to bind and deform dsDNA *in vitro* and to bind cellular DNA in response to activation following elicitor perception. Importantly, while the described biochemistry for Rx1 is novel for a NLR protein, DNA distortion is a well characterized feature of other proteins that interact with DNA through non-sequence specific interactions including TATA box binding protein (78,79), integration host factor (80) and the HMG box (81). Rx1 biochemistry is therefore consistent with the activity of known DNA-binding proteins.

Our observation that Rx1 can interact with DNA in response to immune activation might provide a rationale for its nuclear localisation. For example, a P-loop mutant in Rx1 can potentially establish a correlation between DNA-binding and immunity. The K176R P-loop mutant of Rx1 is defective in triggering immunity (23) to PVX. We show that this mutant is also defective in nucleotide-dependent DNA bending and DNA melting *in vitro*. This finding represents a potential link between the ability of Rx1 to distort DNA *in vitro* to the ability to trigger immunity *in planta*. Equivalent mutations in the NB domain of Cdc6 have been used to investigate the activity of Cdc6 at dsDNA (82,83).

In vivo activation of Rx1 by the PVX coat protein induces the plant immune response (84) (Figure 8B). We found that Rx1 only bound nuclear

DNA following recognition of the CP106 coat protein, but not the CP105 variant, which is unable to trigger Rx1 signalling. These data show that only properly activated Rx1 has the ability to interact with DNA *in situ*. In addition, only cytosolic recognition of CP106, followed by translocation of activated Rx1 to the nucleus, results in full activation of immunity (23). We demonstrate that, even in the presence of the CP106 coat protein, no DNA-binding occurs when Rx1 is artificially retained in either cytosol or nucleus (Figure 8C). This finding presents a potential link between the known spatial requirements for Rx1-mediated immune activation and the DNA-binding observed *in situ*. Such a translocation mechanism might be analogous to that of WHIRLY1, an immune activated transcriptional regulator that translocates to the nucleus and is involved in defence gene expression (85). *In vitro*, full-length (hence mostly inactive) Rx1 purified from *N. benthamiana* did interact with DNA, albeit less strongly than the CC-NBARC form produced in *E. coli* ($Rx1_{1\text{-}489}^{WT}$) (Figure 3E) which is free of the autoinhibitory constraint posed by the LRR domain (86). DNA-binding *in vitro* with full-length Rx1 occurred under conditions where relatively high protein concentrations can be assayed. Presumably Rx1 levels *in vivo* are too low to observe DNA-binding in its non-activated state (Figure 8B). The observed DNA-binding by full-length Rx1 *in situ* is not a generic consequence of plant immunity because activation of immunity through another immune receptor (Pto/AvrPto) did not induce Rx1 DNA-binding. We therefore propose that DNA-binding by Rx1 upon PVX coat protein perception is an essential, specific and early step in the cellular immune response.

The Rx1 NBARC domains share remarkable biochemical properties with the Cdc6/Orc1 family DNA-binding proteins. Rx1 was observed to bind both ssDNA and dsDNA similar to ORC of *Saccharomyces cerevisiae* (87). The Cdc6/Orc1 homology with NLR proteins and the DNA-binding characteristics of the separate PSiP NB and NB-ARC domains, accord with multiple contacts with DNA across both NB and ARC domains. Hence, single point mutations are unlikely to abolish DNA-binding and consistent with previous observations (67) we have not identified point mutations that ablate DNA-binding. Eukaryotic ORCs lack DNA sequence specificity *in vitro* but show higher affinity for specific DNA topologies (88,89). Consistent with this, Rx1 shows higher affinity for branched and melted DNA topologies than for dsDNA. The bend angle introduced into DNA by $Rx1_{1\text{-}489}$ is also of a similar magnitude to that observed in crystal structures of ORC1 from *A. pernix* (45). Analysis of *A. pernix* ORC2 revealed a considerable conformational flexibility stabilized by ATP (54). In this context it is interesting to note that while the bend angle is identical for both wild type and mutant Rx1 proteins in the absence of nucleotide or presence of ADP, the *population* of DNA in the bent state was more prevalent in $Rx1_{1\text{-}489}^{WT}$ supplemented with ATP. The Rx1 activated state is therefore specifically linked to DNA distortion.

The activity of Rx1 on DNA provides biochemical evidence that Rx1 might act as a transcriptional regulator through its NB-ARC domain. DNA-binding by a NLR is a signaling event as the NB-ARC domain is not involved in recognition specificity. Pathogen recognition by NLRs is typically determined by the LRR, often in conjunction with integrated effector targets (90,91). A key process in transcriptional activation is the distortion of DNA to enable the formation of the transcription pre-initiation complex (92-95). In the cell, Rx1 protein might have sequence-specific DNA-binding conferred by interacting protein partners while the NB-ARC domain distorts DNA to a state that activates or represses transcription, depending upon the locus (96). The region encompassing the CC domain, which might interact with DNA via an accessory protein (e.g. a transcription factor) could confer this sequence specificity. The identification of such a binding partner that can confer sequence specificity to the Rx1-DNA interaction represents a significant challenge for the future.

In summary, we have identified a conserved DNA-binding and distorting activity in the NB-ARC domain of the Rx1 protein *in vitro* and link Rx1 activation following elicitor recognition to nuclear DNA binding *in situ*. Rx1 induces cellular immune responses after viral coat protein recognition. We hypothesize that a function for Rx1 is to manipulate DNA into an 'immune-competent' state. The precise nature and role of this Rx1 protein-DNA immune-competent state can now be addressed in future studies.

.

CONFLICT OF INTEREST STATEMENT

The authors declare that they have no conflicts of interest with the contents of this article.

AUTHOR CONTRIBUTIONS

SF, PDT, CHD, GBS, ASEC, EJS, LBW, and FKKG performed the experiments. SF, PDT, CHD, GBS, EJS, GJS, AG, LOP, FLWT, and MJC analysed the data. MRK, GJS, AG, LOP, FLWT, and MJC conceived the experiments. MJC and FLWT conceived the overall project and wrote the manuscript. All authors reviewed the results and approved the final version of the manuscript.

REFERENCES

1. Dangl, J. L., and Jones, J. D. (2001) Plant pathogens and integrated defence responses to infection. *Nature* **411**, 826-833
2. Jones, J. D., and Dangl, J. L. (2006) The plant immune system. *Nature* **444**, 323-329
3. Maekawa, T., Kufer, T. A., and Schulze-Lefert, P. (2011) NLR functions in plant and animal immune systems: so far and yet so close. *Nat Immunol* **12**, 817-826
4. Medzhitov, R. (2007) Recognition of microorganisms and activation of the immune response. *Nature* **449**, 819-826
5. Eitas, T. K., and Dangl, J. L. (2010) NB-LRR proteins: pairs, pieces, perception, partners, and pathways. *Curr Opin Plant Biol* **13**, 472-477
6. Staskawicz, B. J., Mudgett, M. B., Dangl, J. L., and Galan, J. E. (2001) Common and contrasting themes of plant and animal diseases. *Science* **292**, 2285-2289
7. Leipe, D. D., Koonin, E. V., and Aravind, L. (2004) STAND, a class of P-loop NTPases including animal and plant regulators of programmed cell death: multiple, complex domain architectures, unusual phyletic patterns, and evolution by horizontal gene transfer. *J Mol Biol* **343**, 1-28
8. Takken, F. L., and Tameling, W. I. (2009) To nibble at plant resistance proteins. *Science* **324**, 744-746
9. Takken, F. L., Albrecht, M., and Tameling, W. I. (2006) Resistance proteins: molecular switches of plant defence. *Curr Opin Plant Biol* **9**, 383-390
10. van der Biezen, E. A., and Jones, J. D. (1998) The NB-ARC domain: a novel signalling motif shared by plant resistance gene products and regulators of cell death in animals. *Curr Biol* **8**, R226-227
11. Maekawa, T., Cheng, W., Spiridon, L. N., Toller, A., Lukasik, E., Saijo, Y., Liu, P., Shen, Q. H., Micluta, M. A., Somssich, I. E., Takken, F. L., Petrescu, A. J., Chai, J., and Schulze-Lefert, P. (2011) Coiled-coil domain-dependent homodimerization of intracellular barley immune receptors defines a minimal functional module for triggering cell death. *Cell Host Microbe* **9**, 187-199
12. Tameling, W. I., Vossen, J. H., Albrecht, M., Lengauer, T., Berden, J. A., Haring, M. A., Cornelissen, B. J., and Takken, F. L. (2006) Mutations in the NB-ARC domain of I-2 that impair ATP hydrolysis cause autoactivation. *Plant Physiol* **140**, 1233-1245
13. Williams, S. J., Sornaraj, P., Decourcy-Ireland, E., Menz, R. I., Kobe, B., Ellis, J., Dodds, P., and Anderson, P. A. (2011) An autoactive mutant of the M flax rust resistance protein has a preference for binding ATP, while wild-type M protein has a preference for binding ADP. *Mol Plant Microbe Interact* **24**, 897-906
14. Fenyk, S., Campillo Ade, S., Pohl, E., Hussey, P. J., and Cann, M. J. (2012) A nucleotide phosphatase activity in the nucleotide binding domain of an orphan resistance protein from rice. *J Biol Chem* **287**, 4023-4032
15. von Moltke, J., Ayres, J. S., Kofoed, E. M., Chavarria-Smith, J., and Vance, R. E. (2013) Recognition of bacteria by inflammasomes. *Annu Rev Immunol* **31**, 73-106
16. Bernoux, M., Ve, T., Williams, S., Warren, C., Hatters, D., Valkov, E., Zhang, X., Ellis, J. G., Kobe, B., and Dodds, P. N. (2011) Structural and functional analysis of a plant resistance protein TIR domain reveals interfaces for self-association, signaling, and autoregulation. *Cell Host Microbe* **9**, 200-211
17. Rairdan, G. J., Collier, S. M., Sacco, M. A., Baldwin, T. T., Boettrich, T., and Moffett, P. (2008) The coiled-coil and nucleotide binding domains of the Potato Rx disease resistance protein function in pathogen recognition and signaling. *Plant Cell* **20**, 739-751
18. Swiderski, M. R., Birker, D., and Jones, J. D. (2009) The TIR domain of TIR-NB-LRR resistance proteins is a signaling domain involved in cell death induction. *Mol Plant Microbe Interact* **22**, 157-165

19. Burch-Smith, T. M., Schiff, M., Caplan, J. L., Tsao, J., Czymmek, K., and Dinesh-Kumar, S. P. (2007) A novel role for the TIR domain in association with pathogen-derived elicitors. *PLoS Biol* **5**, e68
20. Caplan, J. L., Mamillapalli, P., Burch-Smith, T. M., Czymmek, K., and Dinesh-Kumar, S. P. (2008) Chloroplastic protein NRIP1 mediates innate immune receptor recognition of a viral effector. *Cell* **132**, 449-462
21. Deslandes, L., Olivier, J., Peeters, N., Feng, D. X., Khounlotham, M., Boucher, C., Somssich, I., Genin, S., and Marco, Y. (2003) Physical interaction between RRS1-R, a protein conferring resistance to bacterial wilt, and PopP2, a type III effector targeted to the plant nucleus. *P Natl Acad Sci USA* **100**, 8024-8029
22. Shen, Q. H., Saijo, Y., Mauch, S., Biskup, C., Bieri, S., Keller, B., Seki, H., Ulker, B., Somssich, I. E., and Schulze-Lefert, P. (2007) Nuclear activity of MLA immune receptors links isolate-specific and basal disease-resistance responses. *Science* **315**, 1098-1103
23. Slootweg, E., Roosien, J., Spiridon, L. N., Petrescu, A. J., Tameling, W., Joosten, M., Pomp, R., van Schaik, C., Dees, R., Borst, J. W., Smant, G., Schots, A., Bakker, J., and Goverse, A. (2010) Nucleocytoplasmic distribution is required for activation of resistance by the potato NB-LRR receptor Rx1 and is balanced by its functional domains. *Plant Cell* **22**, 4195-4215
24. Wiermer, M., Germain, H., Cheng, Y. T., Garcia, A. V., Parker, J. E., and Li, X. (2010) Nucleoporin MOS7/Nup88 contributes to plant immunity and nuclear accumulation of defense regulators. *Nucleus* **1**, 332-336
25. Bai, S., Liu, J., Chang, C., Zhang, L., Maekawa, T., Wang, Q., Xiao, W., Liu, Y., Chai, J., Takken, F. L., Schulze-Lefert, P., and Shen, Q. H. (2012) Structure-function analysis of barley NLR immune receptor MLA10 reveals its cell compartment specific activity in cell death and disease resistance. *PLoS pathogens* **8**, e1002752
26. Wirthmueller, L., Zhang, Y., Jones, J. D., and Parker, J. E. (2007) Nuclear accumulation of the Arabidopsis immune receptor RPS4 is necessary for triggering EDS1-dependent defense. *Curr Biol* **17**, 2023-2029
27. Zhu, Z., Xu, F., Zhang, Y., Cheng, Y. T., Wiermer, M., and Li, X. (2010) Arabidopsis resistance protein SNC1 activates immune responses through association with a transcriptional corepressor. *P Natl Acad Sci USA* **107**, 13960-13965
28. Cheng, Y. T., Germain, H., Wiermer, M., Bi, D., Xu, F., Garcia, A. V., Wirthmueller, L., Despres, C., Parker, J. E., Zhang, Y., and Li, X. (2009) Nuclear pore complex component MOS7/Nup88 is required for innate immunity and nuclear accumulation of defense regulators in Arabidopsis. *Plant Cell* **21**, 2503-2516
29. Tameling, W. I., Nooijen, C., Ludwig, N., Boter, M., Slootweg, E., Goverse, A., Shirasu, K., and Joosten, M. H. (2010) RanGAP2 mediates nucleocytoplasmic partitioning of the NB-LRR immune receptor Rx in the Solanaceae, thereby dictating Rx function. *Plant Cell* **22**, 4176-4194
30. Heidrich, K., Wirthmueller, L., Tasset, C., Pouzet, C., Deslandes, L., and Parker, J. E. (2011) Arabidopsis EDS1 connects pathogen effector recognition to cell compartment-specific immune responses. *Science* **334**, 1401-1404
31. Chang, C., Yu, D., Jiao, J., Jing, S., Schulze-Lefert, P., and Shen, Q. H. (2013) Barley MLA immune receptors directly interfere with antagonistically acting transcription factors to initiate disease resistance signaling. *Plant Cell* **25**, 1158-1173
32. Roberts, M., Tang, S., Stallmann, A., Dangl, J. L., and Bonardi, V. (2013) Genetic requirements for signaling from an autoactive plant NB-LRR intracellular innate immune receptor. *PLoS Genet* **9**, e1003465
33. Caplan, J., Padmanabhan, M., and Dinesh-Kumar, S. P. (2008) Plant NB-LRR immune receptors: from recognition to transcriptional reprogramming. *Cell Host Microbe* **3**, 126-135
34. Germain, H., and Seguin, A. (2011) Innate immunity: has poplar made its BED? *New Phytol* **189**, 678-687
35. Yan, N., Chai, J., Lee, E. S., Gu, L., Liu, Q., He, J., Wu, J. W., Kokel, D., Li, H., Hao, Q., Xue, D., and Shi, Y. (2005) Structure of the CED-4-CED-9 complex provides insights into programmed cell death in Caenorhabditis elegans. *Nature* **437**, 831-837
36. Kelley, L. A., and Sternberg, M. J. (2009) Protein structure prediction on the Web: a case study using the Phyre server. *Nat Protoc* **4**, 363-371
37. Karplus, K. (2009) SAM-T08, HMM-based protein structure prediction. *Nucleic Acids Res* **37**, W492-497

38. Emsley, P., Lohkamp, B., Scott, W. G., and Cowtan, K. (2010) Features and development of Coot. *Acta Crystallogr D Biol Crystallogr* **66**, 486-501
39. Winn, M. D., Ballard, C. C., Cowtan, K. D., Dodson, E. J., Emsley, P., Evans, P. R., Keegan, R. M., Krissinel, E. B., Leslie, A. G., McCoy, A., McNicholas, S. J., Murshudov, G. N., Pannu, N. S., Potterton, E. A., Powell, H. R., Read, R. J., Vagin, A., and Wilson, K. S. (2011) Overview of the CCP4 suite and current developments. *Acta Crystallogr D Biol Crystallogr* **67**, 235-242
40. Heo, L., Park, H., and Seok, C. (2013) GalaxyRefine: Protein structure refinement driven by side-chain repacking. *Nucleic Acids Res* **41**, W384-388
41. Schrodinger, LLC. (2010) The PyMOL Molecular Graphics System, Version 1.3r1.
42. Peart, J. R., Lu, R., Sadanandom, A., Malcuit, I., Moffett, P., Brice, D. C., Schauser, L., Jaggard, D. A., Xiao, S., Coleman, M. J., Dow, M., Jones, J. D., Shirasu, K., and Baulcombe, D. C. (2002) Ubiquitin ligase-associated protein SGT1 is required for host and nonhost disease resistance in plants. *P Natl Acad Sci U S A* **99**, 10865-10869
43. Schmidt, T. G., Koepke, J., Frank, R., and Skerra, A. (1996) Molecular interaction between the Strep-tag affinity peptide and its cognate target, streptavidin. *J Mol Biol* **255**, 753-766
44. Westerhof, L. B., Wilbers, R. H., Roosien, J., van de Velde, J., Goverse, A., Bakker, J., and Schots, A. (2012) 3D domain swapping causes extensive multimerisation of human interleukin-10 when expressed in planta. *PLoS One* **7**, e46460
45. Gaudier, M., Schuwirth, B. S., Westcott, S. L., and Wigley, D. B. (2007) Structural basis of DNA replication origin recognition by an ORC protein. *Science* **317**, 1213-1216
46. Sreerama, N., and Woody, R. W. (2000) Estimation of protein secondary structure from circular dichroism spectra: comparison of CONTIN, SELCON, and CDSSTR methods with an expanded reference set. *Anal Biochem* **287**, 252-260
47. Green, V., Curtis, F. A., Sedelnikova, S., Rafferty, J. B., and Sharples, G. J. (2013) Mutants of phage bIL67 RuvC with enhanced Holliday junction binding selectivity and resolution symmetry. *Mol Microbiol* **89**, 1240-1258
48. Grinvald, A., and Steinberg, I. Z. (1974) On the analysis of fluorescence decay kinetics by the method of least-squares. *Anal Biochem* **59**, 583-598
49. Dueber, E. L., Corn, J. E., Bell, S. D., and Berger, J. M. (2007) Replication origin recognition and deformation by a heterodimeric archaeal Orc1 complex. *Science* **317**, 1210-1213
50. Bendahmane, A., Kanyuka, K., and Baulcombe, D. C. (1999) The Rx gene from potato controls separate virus resistance and cell death responses. *Plant Cell* **11**, 781-792
51. Bendahmane, A., Kohn, B. A., Dedi, C., and Baulcombe, D. C. (1995) The coat protein of potato virus X is a strain-specific elicitor of Rx1-mediated virus resistance in potato. *Plant J* **8**, 933-941
52. Albrecht, M., and Takken, F. L. (2006) Update on the domain architectures of NLRs and R proteins. *Biochem Biophys Res Commun* **339**, 459-462
53. Liu, J., Smith, C. L., DeRyckere, D., DeAngelis, K., Martin, G. S., and Berger, J. M. (2000) Structure and function of Cdc6/Cdc18: implications for origin recognition and checkpoint control. *Mol Cell* **6**, 637-648
54. Singleton, M. R., Morales, R., Grainge, I., Cook, N., Isupov, M. N., and Wigley, D. B. (2004) Conformational changes induced by nucleotide binding in Cdc6/ORC from Aeropyrum pernix. *J Mol Biol* **343**, 547-557
55. Chattopadhyaya, R., and Pal, A. (2008) Three-dimensional models of NB-ARC domains of disease resistance proteins in tomato, Arabidopsis, and flax. *J Biomol Struct Dyn* **25**, 357-371
56. Riedl, S. J., Li, W., Chao, Y., Schwarzenbacher, R., and Shi, Y. (2005) Structure of the apoptotic protease-activating factor 1 bound to ADP. *Nature* **434**, 926-933
57. Shrivastava, D., Nain, V., Sahi, S., Verma, A., Sharma, P., Sharma, P. C., and Kumar, P. A. (2011) Insights from molecular modeling and dynamics simulation of pathogen resistance (R) protein from brinjal. *Bioinformation* **5**, 326-330
58. Takken, F. L., and Goverse, A. (2012) How to build a pathogen detector: structural basis of NB-LRR function. *Curr Opin Plant Biol* **15**, 375-384
59. van Ooijen, G., Mayr, G., Kasiem, M. M., Albrecht, M., Cornelissen, B. J., and Takken, F. L. (2008) Structure-function analysis of the NB-ARC domain of plant disease resistance proteins. *J Exp Bot* **59**, 1383-1397

60. Hu, Z., Yan, C., Liu, P., Huang, Z., Ma, R., Zhang, C., Wang, R., Zhang, Y., Martinon, F., Miao, D., Deng, H., Wang, J., Chang, J., and Chai, J. (2013) Crystal structure of NLRC4 reveals its autoinhibition mechanism. *Science* **341**, 172-175
61. Xu, Q., Rife, C. L., Carlton, D., Miller, M. D., Krishna, S. S., Elsliger, M. A., Abdubek, P., Astakhova, T., Chiu, H. J., Clayton, T., Duan, L., Feuerhelm, J., Grzechnik, S. K., Hale, J., Han, G. W., Jaroszewski, L., Jin, K. K., Klock, H. E., Knuth, M. W., Kumar, A., McMullan, D., Morse, A. T., Nigoghossian, E., Okach, L., Oommachen, S., Paulsen, J., Reyes, R., van den Bedem, H., Hodgson, K. O., Wooley, J., Deacon, A. M., Godzik, A., Lesley, S. A., and Wilson, I. A. (2009) Crystal structure of a novel archaeal AAA+ ATPase SSO1545 from Sulfolobus solfataricus. *Proteins* **74**, 1041-1049
62. Sanger, F., Coulson, A. R., Friedmann, T., Air, G. M., Barrell, B. G., Brown, N. L., Fiddes, J. C., Hutchison, C. A., 3rd, Slocombe, P. M., and Smith, M. (1978) The nucleotide sequence of bacteriophage phiX174. *J Mol Biol* **125**, 225-246
63. Yokoyama, H., Kurumizaka, H., Ikawa, S., Yokoyama, S., and Shibata, T. (2003) Holliday junction binding activity of the human Rad51B protein. *J Biol Chem* **278**, 2767-2772
64. Johnson, W. C. (1999) Analyzing protein circular dichroism spectra for accurate secondary structures. *Proteins* **35**, 307-312
65. Gaudreault, M., Gingras, M.-E., Lessard, M., Leclerc, S., and Guerin, S. L. (2009) Electrophoretic mobility shift assays for the analysis of DNA-protein interactions. in *DNA-Protein Interactions: Principles and Protocols* (Moss, T., and Leblanc, B. eds.), Third Ed., Humana Press. pp 15-35
66. Capaldi, S. A., and Berger, J. M. (2004) Biochemical characterization of Cdc6/Orc1 binding to the replication origin of the euryarchaeon Methanothermobacter thermoautotrophicus. *Nucleic Acids Res* **32**, 4821-4832
67. Feng, L., Wang, B., Driscoll, B., and Jong, A. (2000) Identification and characterization of Saccharomyces cerevisiae Cdc6 DNA-binding properties. *Mol Biol Cell* **11**, 1673-1685
68. Harris, C. J., Slootweg, E. J., Goverse, A., and Baulcombe, D. C. (2013) Stepwise artificial evolution of a plant disease resistance gene. *P Natl Acad Sci U S A* **110**, 21189-21194
69. Qi, S., Pang, Y., Hu, Q., Liu, Q., Li, H., Zhou, Y., He, T., Liang, Q., Liu, Y., Yuan, X., Luo, G., Wang, J., Yan, N., and Shi, Y. (2010) Crystal structure of the Caenorhabditis elegans apoptosome reveals an octameric assembly of CED-4. *Cell* **141**, 446-457
70. Grainge, I., Gaudier, M., Schuwirth, B. S., Westcott, S. L., Sandall, J., Atanassova, N., and Wigley, D. B. (2006) Biochemical analysis of a DNA replication origin in the archaeon Aeropyrum pernix. *J Mol Biol* **363**, 355-369
71. Parkhurst, L. J., Parkhurst, K. M., Powell, R., Wu, J., and Williams, S. (2001) Time-resolved fluorescence resonance energy transfer studies of DNA bending in double-stranded oligonucleotides and in DNA-protein complexes. *Biopolymers* **61**, 180-200
72. Gohlke, C., Murchie, A. I., Lilley, D. M., and Clegg, R. M. (1994) Kinking of DNA and RNA helices by bulged nucleotides observed by fluorescence resonance energy transfer. *P Natl Acad Sci USA* **91**, 11660-11664
73. Fujimoto, M., Kuninaka, A., and Yoshino, H. (1974) Studies on a Nuclease from Penicillium-Citrinum .1. Purification of a Nuclease from Penicillium-Citrinum. *Agr Biol Chem Tokyo* **38**, 777-783
74. Cremazy, F. G., Manders, E. M., Bastiaens, P. I., Kramer, G., Hager, G. L., van Munster, E. B., Verschure, P. J., Gadella, T. J., Jr., and van Driel, R. (2005) Imaging in situ protein-DNA interactions in the cell nucleus using FRET-FLIM. *Exp Cell Res* **309**, 390-396
75. Scofield, S. R., Tobias, C. M., Rathjen, J. P., Chang, J. H., Lavelle, D. T., Michelmore, R. W., and Staskawicz, B. J. (1996) Molecular Basis of Gene-for-Gene Specificity in Bacterial Speck Disease of Tomato. *Science* **274**, 2063-2065
76. Spehr, M., Schwane, K., Riffell, J. A., Barbour, J., Zimmer, R. K., Nauhaus, E. M., and Hatt, H. (2004) Particulate adenylate cyclase plays a key role in human sperm olfactory receptor-mediated chemotaxis. *J Biol Chem* **279**, 40194-40203
77. Tang, X., Frederick, R. D., Zhou, J., Halterman, D. A., Jia, Y., and Martin, G. B. (1996) Initiation of Plant Disease Resistance by Physical Interaction of AvrPto and Pto Kinase. *Science* **274**, 2060-2063
78. Kim, J. L., Nikolov, D. B., and Burley, S. K. (1993) Co-crystal structure of TBP recognizing the minor groove of a TATA element. *Nature* **365**, 520-527
79. Kim, Y., Geiger, J. H., Hahn, S., and Sigler, P. B. (1993) Crystal structure of a yeast TBP/TATA-box complex. *Nature* **365**, 512-520

80. Rice, P. A., Yang, S., Mizuuchi, K., and Nash, H. A. (1996) Crystal structure of an IHF-DNA complex: a protein-induced DNA U-turn. *Cell* **87**, 1295-1306
81. Werner, M. H., Huth, J. R., Gronenborn, A. M., and Clore, G. M. (1995) Molecular basis of human 46X,Y sex reversal revealed from the three-dimensional solution structure of the human SRY-DNA complex. *Cell* **81**, 705-714
82. Fernandez-Cid, A., Riera, A., Tognetti, S., Herrera, M. C., Samel, S., Evrin, C., Winkler, C., Gardenal, E., Uhle, S., and Speck, C. (2013) An ORC/Cdc6/MCM2-7 complex is formed in a multistep reaction to serve as a platform for MCM double-hexamer assembly. *Mol Cell* **50**, 577-588
83. Randell, J. C., Bowers, J. L., Rodriguez, H. K., and Bell, S. P. (2006) Sequential ATP hydrolysis by Cdc6 and ORC directs loading of the Mcm2-7 helicase. *Mol Cell* **21**, 29-39
84. Goulden, M. G., Kohm, B. A., Santa Cruz, S., Kavanagh, T. A., and Baulcombe, D. C. (1993) A feature of the coat protein of potato virus X affects both induced virus resistance in potato and viral fitness. *Virology* **197**, 293-302
85. Foyer, C. H., Karpinska, B., and Krupinska, K. (2014) The functions of WHIRLY1 and REDOX-RESPONSIVE TRANSCRIPTION FACTOR 1 in cross tolerance responses in plants: a hypothesis. *Phil Trans R Soc B* **369**, 20130226
86. Slootweg, E. J., Spiridon, L. N., Roosien, J., Butterbach, P., Pomp, R., Westerhof, L., Wilbers, R., Bakker, E., Bakker, J., Petrescu, A. J., Smant, G., and Goverse, A. (2013) Structural determinants at the interface of the ARC2 and leucine-rich repeat domains control the activation of the plant immune receptors Rx1 and Gpa2. *Plant Physiol* **162**, 1510-1528
87. Lee, D. G., Makhov, A. M., Klemm, R. D., Griffith, J. D., and Bell, S. P. (2000) Regulation of origin recognition complex conformation and ATPase activity: differential effects of single-stranded and double-stranded DNA binding. *Embo J* **19**, 4774-4782
88. MacAlpine, H. K., Gordan, R., Powell, S. K., Hartemink, A. J., and MacAlpine, D. M. (2010) Drosophila ORC localizes to open chromatin and marks sites of cohesin complex loading. *Genome Res* **20**, 201-211
89. Remus, D., Beall, E. L., and Botchan, M. R. (2004) DNA topology, not DNA sequence, is a critical determinant for Drosophila ORC-DNA binding. *Embo J* **23**, 897-907
90. Cesari, S., Bernoux, M., Moncuquet, P., Kroj, T., and Dodds, P. N. (2014) A novel conserved mechanism for plant NLR protein pairs: the "integrated decoy" hypothesis. *Front Plant Sci* **5**, 606
91. Wu, C. H., Krasileva, K. V., Banfield, M. J., Terauchi, R., and Kamoun, S. (2015) The "sensor domains" of plant NLR proteins: more than decoys? *Front Plant Sci* **6**, 134
92. Finzi, L., and Dunlap, D. D. (2010) Single-molecule approaches to probe the structure, kinetics, and thermodynamics of nucleoprotein complexes that regulate transcription. *J Biol Chem* **285**, 18973-18978
93. Kim, H., Tang, G. Q., Patel, S. S., and Ha, T. (2012) Opening-closing dynamics of the mitochondrial transcription pre-initiation complex. *Nucleic Acids Res* **40**, 371-380
94. Liu, X., Bushnell, D. A., Wang, D., Calero, G., and Kornberg, R. D. (2010) Structure of an RNA polymerase II-TFIIB complex and the transcription initiation mechanism. *Science* **327**, 206-209
95. Tang, G. Q., Deshpande, A. P., and Patel, S. S. (2011) Transcription factor-dependent DNA bending governs promoter recognition by the mitochondrial RNA polymerase. *J Biol Chem* **286**, 38805-38813
96. Fogg, J. M., Randall, G. L., Pettitt, B. M., Sumners de, W. L., Harris, S. A., and Zechiedrich, L. (2012) Bullied no more: when and how DNA shoves proteins around. *Q Rev Biophys* **45**, 257-299

Acknowledgments- We would like to thank Sarah Peyton for help with method development, Rikus Pomp for technical support and helpful advice, and Martijn Rep for critical feedback on the manuscript.

FOOTNOTES

* This work was supported by BBSRC grant BB/I011994/1 to MJC, GJS and MRK, EU-funded Integrated Project BIOEXPLOIT to AG, EJS, FLWT and FKKG, and Top Technology Institute Green Genetics and the Dutch Science Foundation for Earth and Life Sciences to AG and LBW.

[1]School of Biological and Biomedical Sciences, [2]Biophysical Sciences Institute, [3]Department of Chemistry, Durham University, South Road, Durham, DH1 3LE, United Kingdom. [4]Laboratory of Nematology, Department of Plant Sciences, Wageningen University, 6708 PB, Wageningen, The Netherlands. [5]Molecular Plant Pathology, Swammerdam Institute for Life Sciences, University of Amsterdam, Science Park 904, 1098 XH, Amsterdam, The Netherlands. [6] These authors contributed equally to this work

[7] The abbreviations used are: AAA+, ATPases associated with diverse cellular activities; CC, coiled-coil; EMSA, Electrophoretic mobility shift assays; FLIM, Fluorescence lifetime imaging microscopy; FRET, Fluorescence resonance energy transfer; NB, nucleotide-binding; NB-ARC, Nucleotide-Binding, Apaf-1, R-proteins, and CED-4; LRR, leucine-rich repeat; NES, nuclear export sequence; NLS, nuclear localisation sequence; NLR, nucleotide-binding leucine-rich repeat; PSiP, Polled-Signaling Protein; PVX, Protein Virus X; STAND, signal-transduction ATPases with numerous domains; TIR, Toll–interleukin 1 receptor.

FIGURE LEGENDS

Figure 1. Structural modeling of the Rx1 NB-ARC domains. **A.** Alignment of Rx1 (residues 134-479) with Orc1 of *Aeropyrum pernix* (PDB 2V1U; residues 13-382). Numbers denote amino acid residue position. Sequences are in standard single letter amino acid code and functionally related residues between the two proteins are indicated by a colon. The Rx1 domain structure is denoted by a colored line above the Rx1 sequence and corresponds to the NB (green), ARC1 (red), and ARC2 (blue) domains. Residues in light blue contact DNA bases in the Orc1-DNA structure, whereas those in red contact DNA bases and/or the DNA backbone (45, 49). Known (Orc1) and predicted (Rx1) secondary structures (α-helix (yellow) or β-sheet (grey)) are indicated. (**B**) Structural homology model for Rx1 based on the crystal structure of DNA-bound Cdc6/Orc1 from *Aeropyrum pernix*. Left panel: structural homology model of the NB-ARC domain of Rx1 (amino acids 143-4780, with associated ADP (NB domain (green), ARC1 domain (red), ARC2 (blue)). Centre panel, crystal structure of *Aeropyrum pernix* Cdc6/Orc1 in complex with DNA (PDB 2V1U) (pink: amino acids 13-279, yellow: amino acids 280-399). Right panel, crystal structure for Cdc6/Orc1 of *Pyrobaculum aerophilum* not bound to DNA (PDB 1FNN) (pink: amino acids 1-278, yellow: amino acids 279-388). (**C**) Comparison of the PDB 2V1U-based Rx1 homology model with the crystal structure of Cdc6/Orc1 of *P. aerophilum* (PDB 1FNN). Left panel: complete overlay of both structures. Note that only the NB (green) and ARC1 (red) superimposes and that the ARC2 domain (blue) of Rx1 is rotated compared to the C-terminal region of Cdc6/Orc1 of *P. aerophilum* (yellow). Centre panel: overlay highlighting the C-terminal ARC1 (red) and ARC2 (blue) domains of Rx1. Right panel: superposition of the C-terminal domain of Cdc6/Orc1 of *P. aerophilum* onto the Rx1 model. Domain designation is as for panel (B).

Figure 2. Production and characterization of a recombinant Rx1 protein. (**A**) Purified Rx1 protein (1.5 μg) was separated by 12.5% SDS-PAGE gel electrophoresis and stained with Coomassie blue. Molecular mass standards (in kDa) are indicated. Protein identity was confirmed by trypsin digest and MALDI-TOF analysis. A circular dichroism spectrum for (**B**) $Rx1_{1\text{-}479}^{WT}$ and (**C**) $Rx1_{1\text{-}479}^{K176R}$ depicting experimental data (green dots) and the spectrum calculated using CDSSTR (grey dots).

Figure 3. The Rx1 CC-NBARC domains bind nucleic acids *in vitro.* (**A**) EMSA for $Rx1_{1\text{-}489}^{WT}$, $Rx1_{1\text{-}489}^{K176R}$ and BSA using 100 ng ϕX174 virion DNA (ssDNA) or ϕX174 virion RF I DNA (dsDNA). For dsDNA the upper band represents relaxed circular DNA while the lower band represents supercoiled circular DNA. (**B-D**) Upper panels: Representative EMSA for $Rx1_{1\text{-}479}^{WT}$ showing raw data for binding to nucleic acids. Lower panels: Quantitative EMSA analysis giving apparent affinities of $Rx1_{1\text{-}489}^{WT}$ and $Rx1_{1\text{-}489}^{K176R}$ for dsDNA (**B**), ssRNA (**C**) and ssDNA (**D**) (n=3-6, ±S.E.M). (**E**) Quantitative EMSA showing binding of 1 mM full-length plant-expressed strep tagged Rx1 (Rx1-4Strep), *E. coli* produced $Rx1_{1\text{-}489}^{WT}$, or BSA to ssDNA (n=8, ±S.E.M. bars with different letters are significantly different ($p<0.05$), one-way ANOVA with post-hoc Tukey's multiple comparison). (**F**) Quantitative EMSA analysis giving comparative affinities of PSiP-NB-ARC and PSiP-NB for ssDNA (n=3, ±S.E.M).

Figure 4. $Rx1_{1\text{-}489}$ bends dsDNA. (**A**) Double stranded DNA-binding by $Rx1_{1\text{-}489}^{WT}$ and $Rx1_{1\text{-}489}^{K176R}$ assessed by EMSA plotted as a ratio of binding in the presence of 1 μM nucleotide compared to no nucleotide (n=3, ±S.E.M., a $p>0.05$). The used DNA is identical to that used for Figure 3B. (**B**) Sample time-resolved data for a control (No protein) and $Rx_{1\text{-}489}^{WT}$ with and without ATP. The data shows fluorescent counts from the fluorescent donor plotted against time. The appropriate colour arrowhead indicates the 129 ps lifetime associated with energy transfer. (**C**) The percentage contribution of the 129 ps lifetime for fluorescent donor in the presence of BSA or $Rx1_{1\text{-}489}$ and nucleotides (D-only donor labeled oligonucleotide only, no protein; D/A-donor and acceptor labeled oligonucleotide, no protein) (n=3-11, ±S.E.M. bars with different letters are significantly different ($p<0.05$), one-way ANOVA with post-hoc Tukey's multiple comparison).

Figure 5. $Rx1_{1\text{-}489}$ induces localized DNA melting. DNA remaining undigested after treatment with P_1 nuclease in the presence of BSA, $Rx1_{1\text{-}489}^{WT}$, $Rx1_{1\text{-}489}^{K176R}$, or ORC as a percentage of total DNA (n=6-19, ±S.E.M. * $p<0.05$ compared to dsDNA in the presence of BSA by one-way ANOVA with post-hoc Dunnett

test). The inset panel shows a control EMSA using the C3/mORB dual-site DNA sequence at *oriC2* of *Sulfolobus solfataricus* in the presence or absence of 1.5 mM ORC.

Figure 6. Rx1 preferentially binds distorted DNA topologies. (**A**) Quantitative EMSA analysis giving comparative affinities of $Rx1_{1\text{-}489}^{WT}$ for ssDNA (ssF12), dsDNA (dsF12), branched dsDNA with two dsDNA arms (F12-ds/ds), branched dsDNA with two ssDNA arms (F12-ss/ss), and branched dsDNA with one ssDNA and one dsDNA arm (F12-ds/ss) (*n*=3-4, ±S.E.M). (**B**) Quantitative EMSA analysis giving comparative affinities of $Rx1_{1\text{-}489}^{WT}$ for ssDNA (ssP1), dsDNA (dsP1), and dsDNA with bubbles of varying sizes (*n*=3-4, ±S.E.M).

Figure 7. Individual fluorescent lifetime signals for GFP can be resolved from agroinfiltrated plants. (**A**) Plot of the identified fluorescent lifetimes for GFP from agroinfiltrated *Nicotiana benthamiana* epithelial cell nuclei against the percentage yield for that lifetime. The graph represents 14 measurements from 7 independently infiltrated leaves with each measurement proving two fluorescent lifetime values. (**B**) Ratios for the integrated emission intensities for GFP and LDS 751 in GFP (negative control) and H2B-GFP (positive control) agroinfiltrated *N. benthamiana* (*n*=6-7; bars with different letters are significantly different ($p<0.05$), Student's T-test).

Figure 8. Binding of Rx1 protein domains to DNA *in situ.* (**A**) The ratio of the long (>1.0 ns) to short (<0.5 ns) GFP lifetimes for GFP fusion constructs representing varying Rx1 subdomains produced in *N. benthamiana* leaves using agroinfiltration (*n*>6; * $p<0.05$ compared to GFP by one-way ANOVA with post-hoc Dunnett test). (**B**) The ratio of the long (>1.0 ns) to short (<0.5 ns) GFP lifetimes for Rx1-GFP full-length constructs alone and upon co-expression with virulent (CP105) and avirulent alleles (CP106) of the PVX CP (*n*>6; * $p<0.05$ compared to GFP by one-way ANOVA with post-hoc Dunnett test). (**C**) The ratio of the long (>1.0 ns) to short (<0.5 ns) GFP lifetimes for GFP-NLS-Rx1 and GFP-NES-Rx1 full-length constructs alone and upon co-expression with the avirulent allele of PVX, CP106 (*n*=4; * $p<0.05$ compared to GFP by one-way ANOVA with post-hoc Dunnett test). (**D**) The ratio of the long (>1.0 ns) to short (<0.5 ns) GFP lifetimes for Rx1-GFP full-length construct alone and upon co-expression with either the avirulent allele of PVX, CP106, or the Pto kinase and AvrPto (*n*=12-20, * $p<0.05$ compared to GFP by one-way ANOVA with post-hoc Dunnett test).

TABLE 1 Apparent dissociation constants for recombinant NLR domain interactions with nucleic acids. Error values represent the standard deviation.

Protein	**K_d^{app} ssDNA [mM]**	**K_d^{app} dsDNA [mM]**	**K_d^{app} ssRNA [mM]**
$Rx_{1\text{-}489}^{WT}$	0.014±0.002	0.70±0.05	0.20±0.03
$Rx_{1\text{-}489}^{K176R}$	0.036±0.004	5.69±0.85	0.77±0.09
PSiP-NB	>50	ND	ND
PSiP-NB-ARC	4.08±0.26	ND	ND

Figure 1

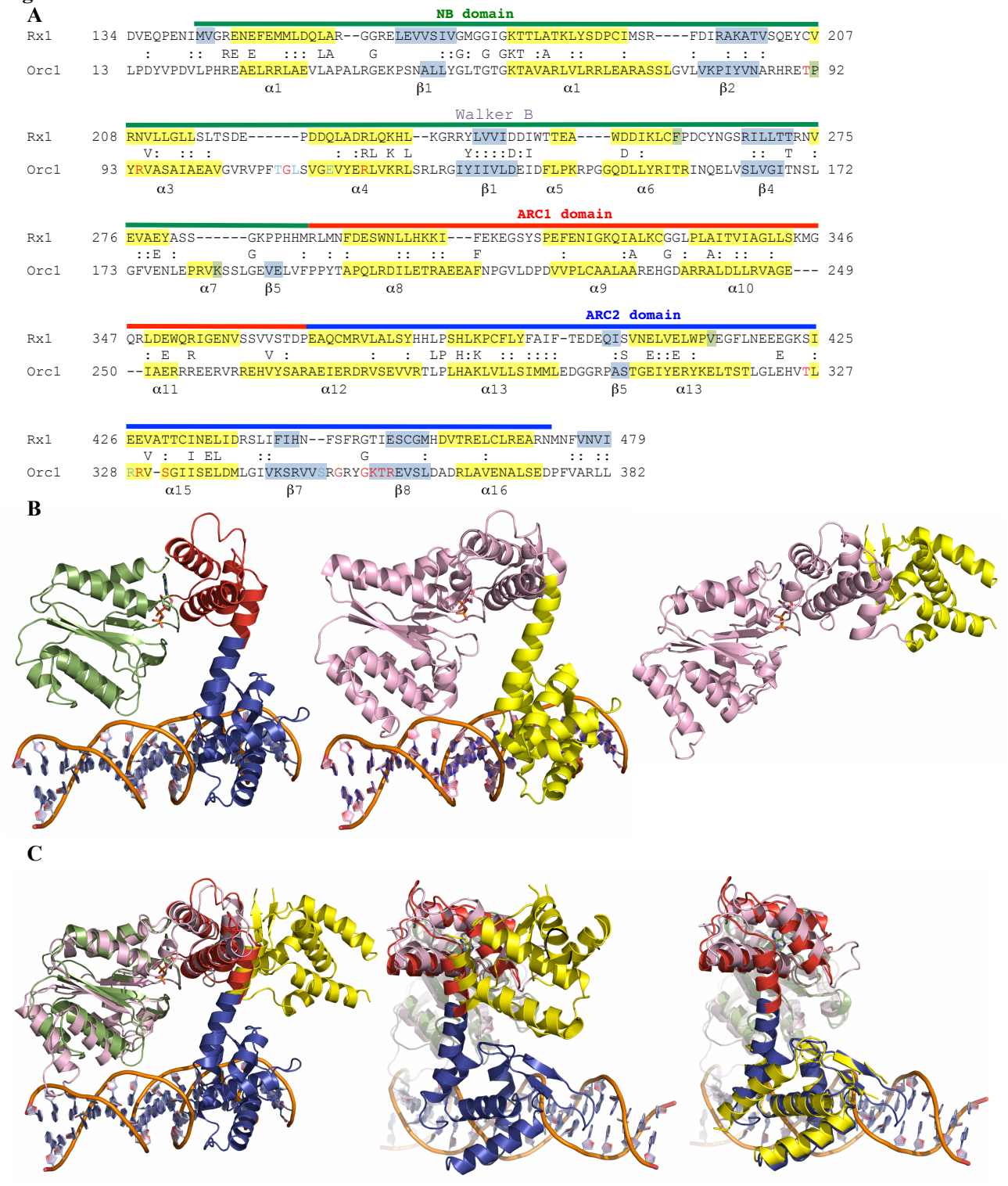

Figure 2

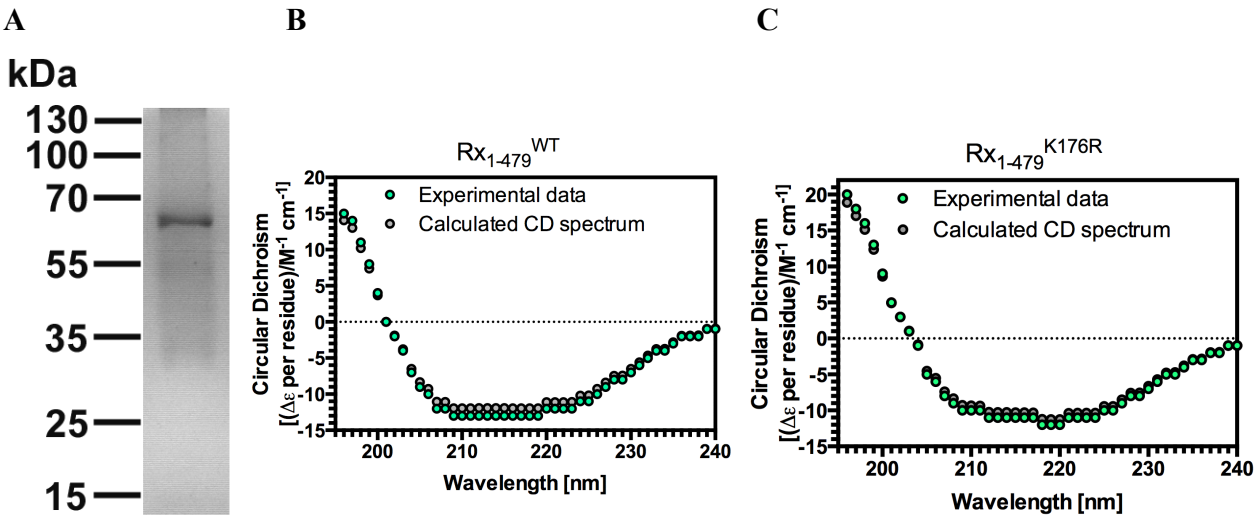

Figure 3

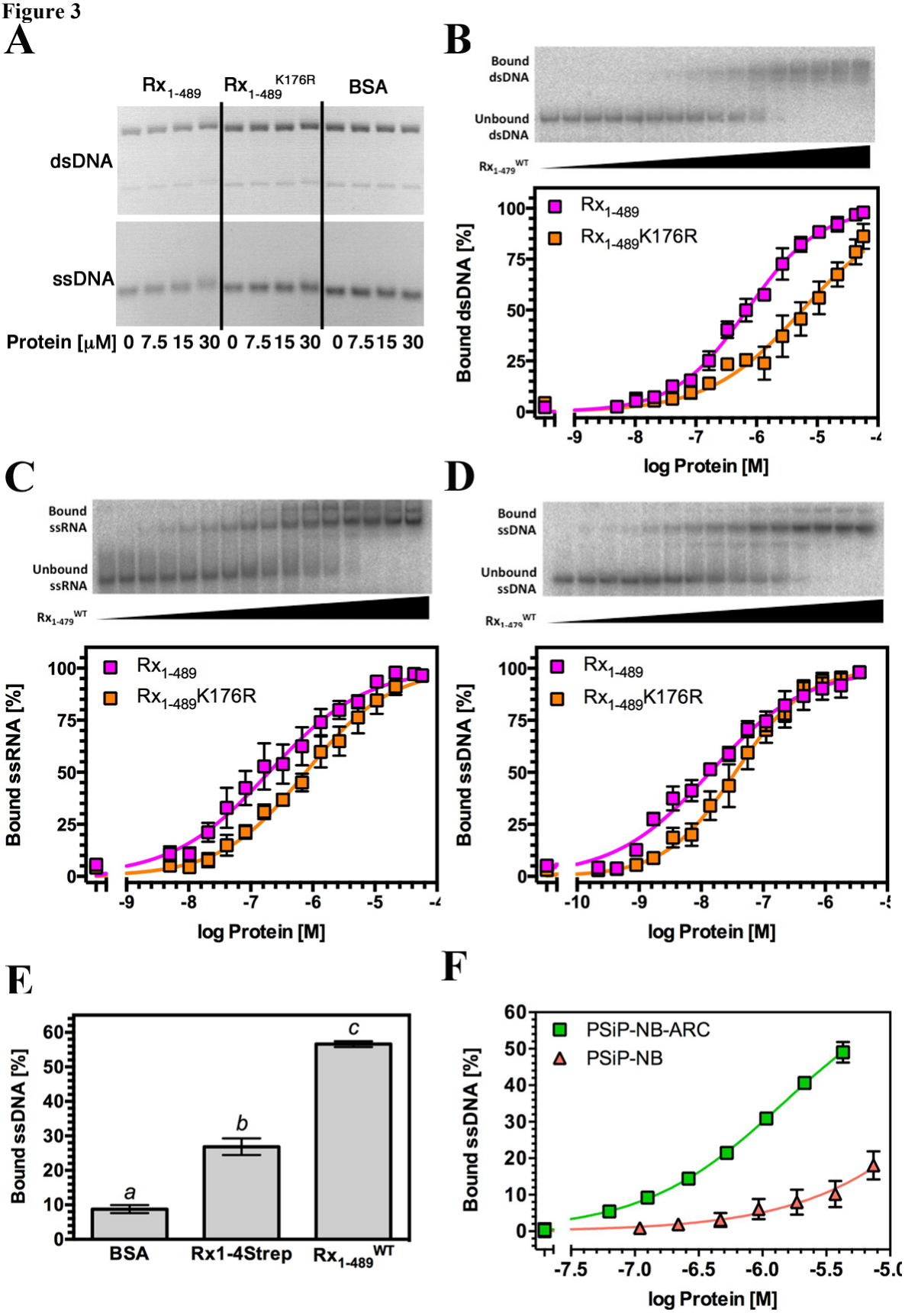

Figure 4

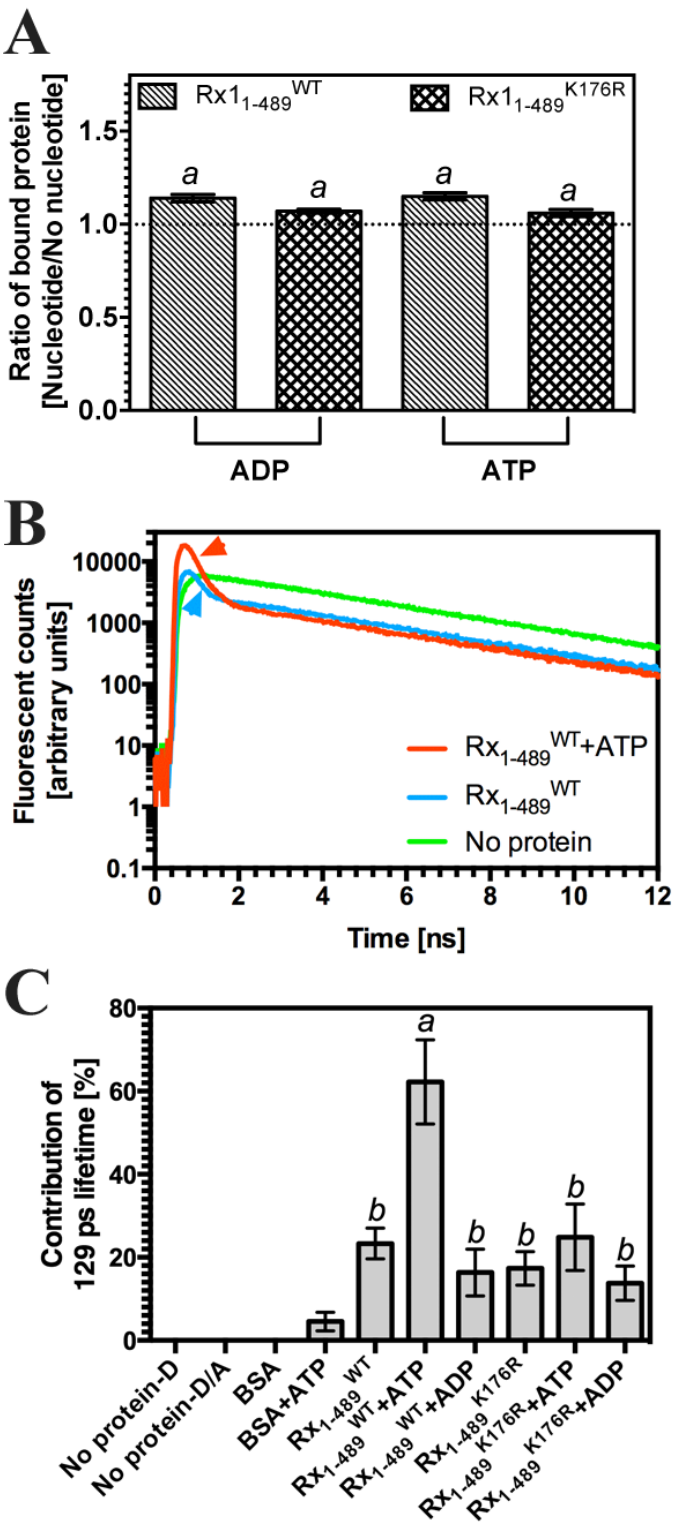

Figure 5

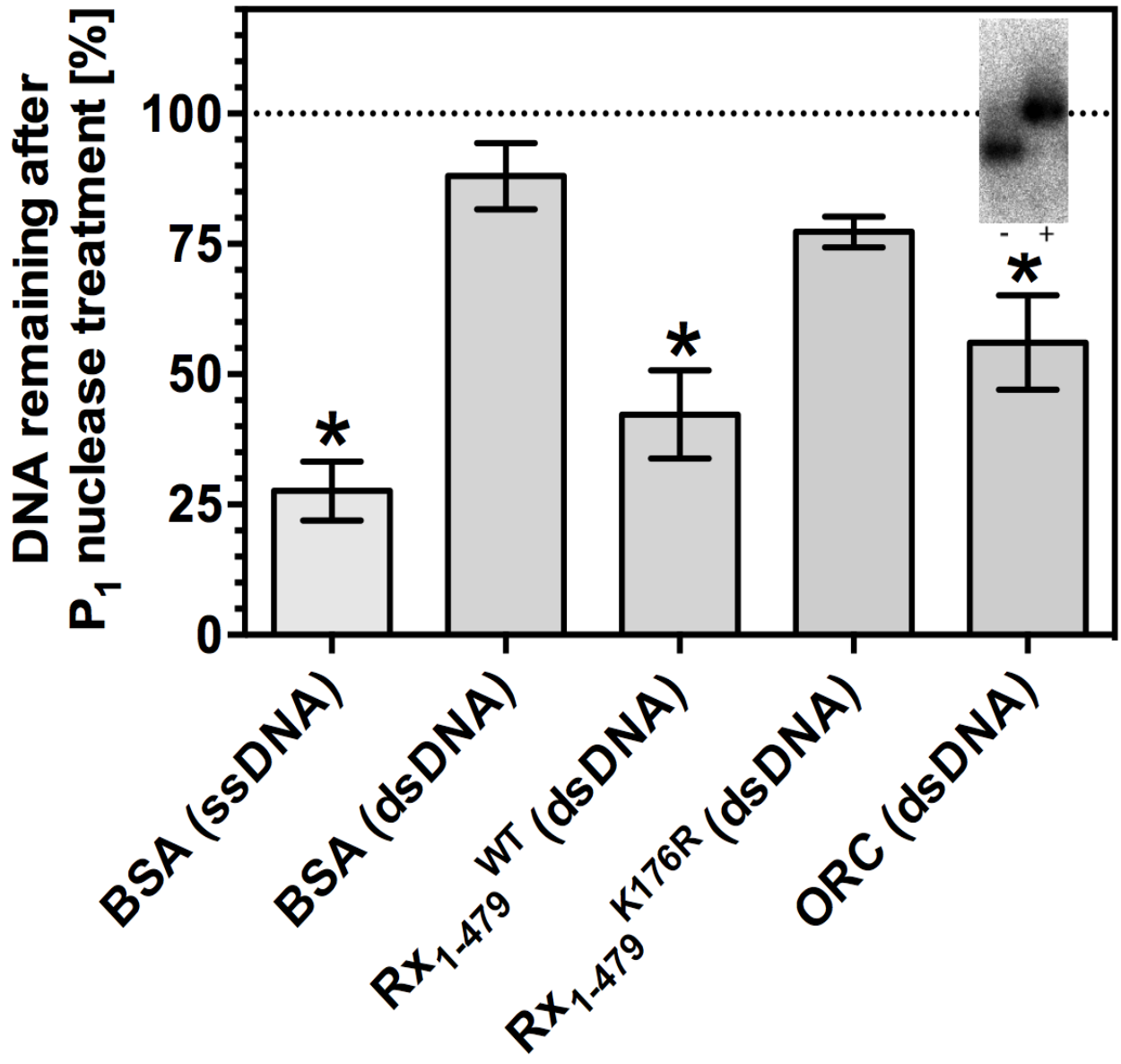

Figure 6

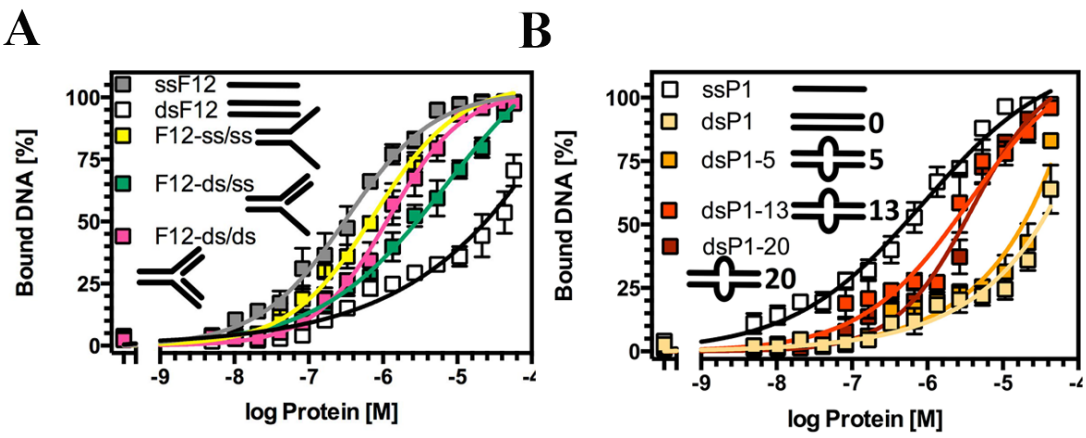

Figure 7

A

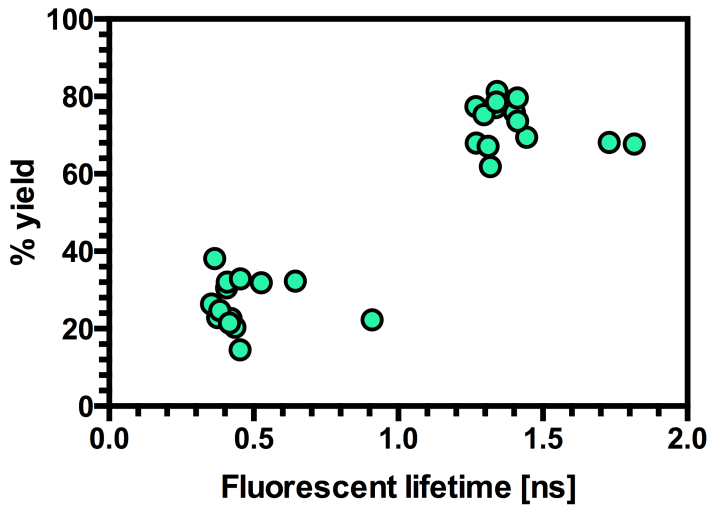

B

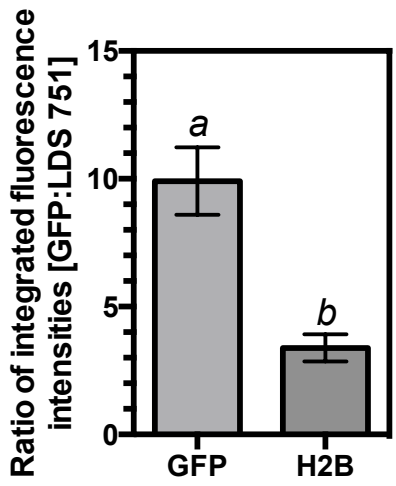

Figure 8.

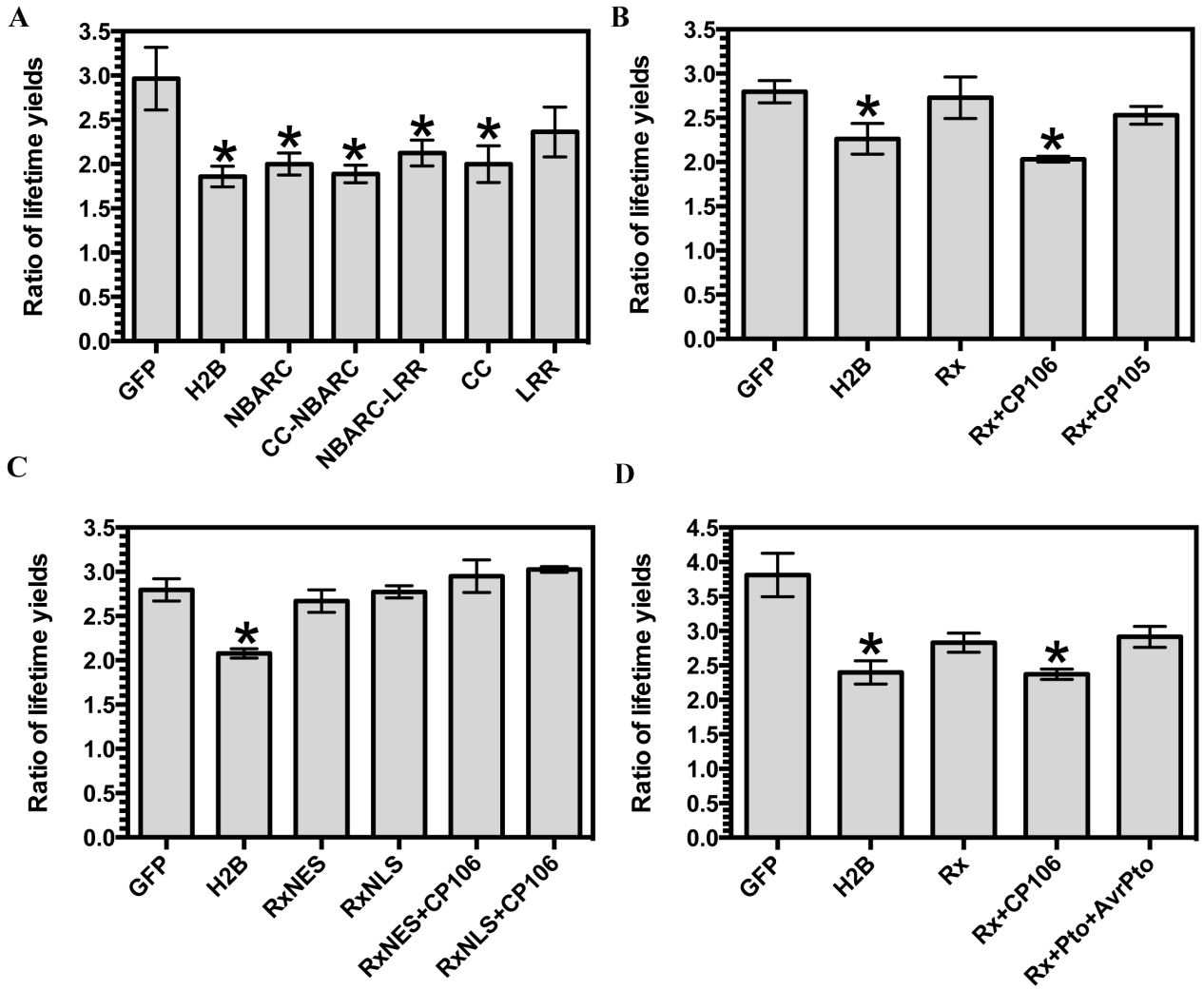

Plant Biology:

The Potato Nucleotide-Binding Leucine-Rich Repeat (NLR) Immune Receptor Rx1 is a Pathogen Dependent DNA-Deforming Protein

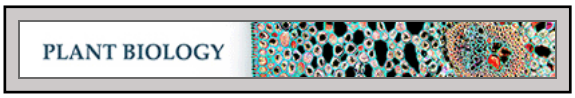

Stepan Fenyk, Philip D. Townsend, Christopher H. Dixon, Gerhard B. Spies, Alba de San Eustaquio Campillo, Erik J. Slootweg, Lotte B. Westerhof, Fleur K. K. Gawehns, Marc R. Knight, Gary J. Sharples, Aska Goverse, Lars-Olof Pålsson, Frank L. W. Takken and Martin J. Cann

J. Biol. Chem. published online August 25, 2015